

The Oscillation Probability of GeV Solar Neutrinos of All Active Species

André de Gouvêa

*CERN - Theory Division
CH-1211 Geneva 23, Switzerland*

Abstract

In this paper, I address the oscillation probability of $O(\text{GeV})$ neutrinos of all active flavours produced inside the Sun and detected at the Earth. Flavours other than electron-type neutrinos may be produced, for example, by the annihilation of WIMPs which may be trapped inside the Sun. In the GeV energy regime, matter effects are important both for the “1–3” system and the “1–2” system, and for different neutrino mass hierarchies. A numerical scan of the multidimensional three-flavour parameter space is performed, “inspired” by the current experimental situation. One important result is that, in the three-flavour oscillation case, $P_{\alpha\beta} \neq P_{\beta\alpha}$ for a significant portion of the parameter space, even if there is no CP -violating phase in the MNS matrix. Furthermore, $P_{\mu\mu}$ has a significantly different behaviour from $P_{\tau\tau}$, which may affect expectations for the number of events detected at large neutrino telescopes.

1 Introduction

In the Standard Model of particle physics, neutrinos are strictly massless. Any evidence for neutrino masses would, therefore, imply physics beyond the Standard Model. Even though the direct experimental determination of a neutrino mass is (probably) far beyond the current experimental reach, experiments have been able to obtain indirect, and recently very strong, evidence for neutrino masses, via neutrino oscillations.

The key evidence for neutrino oscillations comes from the angular dependent flux of atmospheric muon-type neutrinos measured at SuperKamiokande [1], combined with a large deviation of the muon-type to electron-type neutrino flux ratio from theoretical predictions. This “atmospheric neutrino puzzle” is best solved by assuming that ν_μ oscillates into ν_τ and that the ν_e does not oscillate. For a recent analysis of all the atmospheric neutrino data see [2].

On the other hand, measurements of the solar neutrino flux [3, 4, 5, 6, 7] have always been plagued by a large suppression of the measured solar ν_e flux with respect to theoretical predictions [8]. Again, this “solar neutrino puzzle” is best resolved by assuming that ν_e oscillates into a linear combination of the other flavour eigenstates [9, 10] (for a more conservative analysis of the event rates and the inclusion of the “dark side” of the parameter space, see [11]). The most recent analysis of the solar neutrino data which includes the mixing of three active neutrino species can be found in [12].

Neutrino oscillations were first hypothesised by Bruno Pontecorvo in the 1950’s [13]. The hypothesis of three flavour mixing was first raised by Maki, Nakagawa and Sakata [14]. In light of the solar neutrino puzzle, Wolfenstein [15] and Mikheyev and Smirnov [16] realized that neutrino–matter interactions could affect in very radical ways the survival probability of electron-type neutrinos which are produced in the solar core and detected at the Earth (MSW effect).

Since then, significant effort has been devoted to understanding the oscillation probabilities of electron-type neutrinos produced in the Sun. For example, in [17] the survival probability of solar electron-type neutrinos was discussed in the context of three-neutrino mixing including matter effects, and solutions to the solar neutrino puzzle in this context were studied (for example, in [17, 18, 12]).

In this paper, the understanding of solar neutrino oscillations is extended to the case of other active neutrino species (ν_μ , ν_τ , and antineutrinos) produced

in the solar core. Even though only electron-type neutrinos are produced by the nuclear reactions which take place in the Sun's innards, it is well known that, in a number of dark matter models, dark matter particles can be trapped gravitationally inside the Sun, and that the annihilation of these should yield a flux of high energy neutrinos ($E_\nu \gtrsim 1$ GeV) of all species which may be detectable at the Earth [19]. Indeed, this is one of the goals of very large “neutrino telescopes,” such as AMANDA [20] or BAIKAL [21]. It is important to understand how neutrino oscillations will affect the expected event rates at these experiments.*

The oscillation probability of all neutrino species has, of course, been studied in different contexts, such as in the case of neutrinos produced in the core of supernovae [23] or in the case of neutrinos propagating in constant electron number densities [24]. The latter case has been receiving a considerable amount of attention from neutrino factory studies [25]. The case at hand (GeV solar neutrinos) differs significantly from these mentioned above, in at least a few of the following: source-detector distance, electron number density average value and position dependency, energy average value and spectrum. Neutrino factory studies, for example, are interested in $O(1000)$ km baselines, $O(10)$ GeV electron-type and muon-type neutrinos produced via muon decay propagating in roughly constant, Earth-like (matter densities around 3 g/cm^3) electron number densities.

The paper is organised as follows. In Sec. 2, the well known case of two-flavour oscillations is reviewed in some detail, while special attention will be paid to neutrinos produced inside the Sun. In Sec. 3 the same discussion is extended to the less familiar case of three-flavour oscillations. Again, special attention is paid to neutrinos produced in the Sun's core. In Sec. 4 the results presented in Sec. 3 will be analysed numerically, and the three-neutrino multi-dimensional parameter space will be explored. Sec. 5 contains a summary of the results and the conclusions.

It is important to comment at this point that one of the big challenges of studying three-flavour oscillations is the multi-dimensional parameter space, composed of three mixing angles, two mass-squared differences, and one complex phase, plus the neutrino energy. For this reason, the discussions presented here will take advantage of the current experimental situation to constrain the parameter space, and of the possibility of producing neutrinos of all species via dark matter annihilations to constrain the neutrino energies

*Some effects have already been studied, in the two-neutrino case, in [22].

to the range from a few to tens of GeV.

2 Two-Flavour Oscillations

In this section, the well studied case of two-flavour oscillations will be reviewed [26]. This is done in order to present the formalism which will be later extended to the case of three-flavour oscillations and describe general properties of neutrino oscillations and of neutrinos produced in the Sun's core.

2.1 Generalities

Neutrino oscillations take place because, similar to what happens in the quark sector, neutrino weak eigenstates are different from neutrino mass eigenstates. The two sets are related by a unitary matrix, which is, in the case of two-flavour mixing, parametrised by one mixing angle ϑ .[†]

$$\begin{pmatrix} \nu_e \\ \nu_x \end{pmatrix} = \begin{pmatrix} U_{e1} & U_{e2} \\ U_{x1} & U_{x2} \end{pmatrix} \begin{pmatrix} \nu_1 \\ \nu_2 \end{pmatrix} = \begin{pmatrix} \cos \vartheta & \sin \vartheta \\ -\sin \vartheta & \cos \vartheta \end{pmatrix} \begin{pmatrix} \nu_1 \\ \nu_2 \end{pmatrix}, \quad (2.1)$$

where ν_1 and ν_2 are neutrino mass eigenstates with masses m_1 and m_2 , respectively, and ν_x is the flavour eigenstate orthogonal to ν_e . All physically distinguishable situations can be obtained if $0 \leq \vartheta \leq \pi/2$ and $m_1^2 \leq m_2^2$ or $0 \leq \vartheta \leq \pi/4$ and no constraint is imposed on the masses-squared.

In the case of oscillations in vacuum, it is trivial to compute the probability that a neutrino produced in a flavour state α is detected as a neutrino of flavour β , assuming that the neutrinos are ultrarelativistic and propagate with energy E_ν :

$$P_{\alpha\beta} = |U_{\beta 1}|^2 |U_{\alpha 1}|^2 + |U_{\beta 2}|^2 |U_{\alpha 2}|^2 + 2 \operatorname{Re} \left(U_{\beta 1}^* U_{\beta 2} U_{\alpha 1} U_{\alpha 2}^* e^{i \frac{\Delta m^2 x}{2E_\nu}} \right). \quad (2.2)$$

Here $\Delta m^2 \equiv m_2^2 - m_1^2$ is the mass-squared difference between the two mass eigenstates and x is the distance from the detector to the source. It is trivial to note that $P_{\alpha\beta} = P_{\beta\alpha}$ since all $U_{\alpha i}$ are real and the theory is T -conserving. Furthermore, note that ϑ is indistinguishable from $\pi/2 - \vartheta$ (or, equivalently,

[†]If the neutrinos are Majorana particles, there is also a Majorana phase, which will be ignored throughout since it plays no role in the physics of neutrino oscillations.

the sign of Δm^2 is not physical), and all physically distinguishable situations are obtained by allowing $0 \leq \vartheta \leq \pi/4$ and choosing a fixed sign for Δm^2 .

In the case of nontrivial neutrino–medium interactions, the computation of $P_{\alpha\beta}$ can be rather involved. Assuming that the neutrino–medium interactions can be expressed in terms of an effective potential for the neutrino propagation, one has to solve

$$\frac{d}{dt} \begin{pmatrix} \nu_1(t) \\ \nu_2(t) \end{pmatrix} = -i \left[\begin{pmatrix} E_1 & 0 \\ 0 & E_2 \end{pmatrix} + \begin{pmatrix} V_{11}(t) & V_{12}(t) \\ V_{12}(t)^* & V_{22}(t) \end{pmatrix} \right] \begin{pmatrix} \nu_1(t) \\ \nu_2(t) \end{pmatrix}, \quad (2.3)$$

with the appropriate boundary conditions (either a ν_e or a ν_x as the initial state, for example). In the ultrarelativistic limit one may approximate $E_2 - E_1 \simeq \Delta m^2/2E_\nu$, $d/dt \simeq d/dx$, and $V_{ij}(t) \simeq V_{ij}(x)$. A very crucial assumption is that there is no kind of neutrino absorption due to the neutrino–medium interaction, *i.e.*, the 2×2 Hamiltonian for the neutrino system is Hermitian.

It is interesting to argue what can be said about $P_{\alpha\beta}$ in very general terms. First, the conservation of probability requires that

$$P_{ee} + P_{ex} = 1, \quad (2.4)$$

$$P_{xe} + P_{xx} = 1. \quad (2.5)$$

Second, given that the Hamiltonian evolution is unitary,

$$P_{ee} + P_{xe} = 1. \quad (2.6)$$

It is easy to show that the extra constraint $P_{ex} + P_{xx} = 1$ is redundant. Eq. (2.6) can be understood by the following “intuitive” argument: if the same amount of ν_e and ν_x is produced, independent of what happens to ν_e and ν_x during flight, the number of ν_e and ν_x detected in the end has to be the same. In light of the constraints above, one can show that there is only one independent $P_{\alpha\beta}$, which is normally chosen to be P_{ee} . The others are given by $P_{ex} = P_{xe} = 1 - P_{ee}$ and $P_{xx} = P_{ee}$. Note that the equality $P_{ex} = P_{xe}$ is *not* a consequence of T -invariance, but a consequence of the unitarity of the Hamiltonian evolution and particular only to the two-flavour oscillation case, as will be shown later.

2.2 Oscillation of Neutrinos Produced in the Sun’s Core

It is well known [15, 16] that neutrino–Sun interactions affect the oscillation probabilities of neutrinos produced in the Sun’s core in very nontrivial ways.

Indeed, all but one solution to the solar neutrino puzzle rely heavily on neutrino–Sun interactions [9, 10, 11]. The survival probability of electron-type solar neutrinos has been computed in many different approximations by a number of people over the years, and can be understood in very simple terms [26].

In the presence of electrons, the differential equation satisfied by the two neutrino system is, in the flavour basis,

$$\frac{d}{dx} \begin{pmatrix} \nu_e(x) \\ \nu_x(x) \end{pmatrix} = -i \left[\frac{\Delta m^2}{2E_\nu} \begin{pmatrix} |U_{e2}|^2 & U_{e2}^* U_{\mu 2} \\ U_{e2} U_{\mu 2}^* & |U_{\mu 2}|^2 \end{pmatrix} + \begin{pmatrix} A(x) & 0 \\ 0 & 0 \end{pmatrix} \right] \begin{pmatrix} \nu_e(x) \\ \nu_x(x) \end{pmatrix}, \quad (2.7)$$

where terms proportional to the 2×2 identity matrix were neglected, since they play no role in the physics of neutrino oscillations.

$$A(x) = \sqrt{2} G_F N_e(x) \quad (2.8)$$

is the charged current contribution to the ν_e – e forward scattering amplitude, G_F is Fermi’s constant, and $N_e(x)$ is the position dependent electron number density. In the case of the Sun [8] (see also [27]), $A \equiv A(0) \simeq 6 \times 10^{-3} \text{ eV}^2/\text{GeV}$, assuming an average core density of 79 g/cm^3 , and $A(x)$ falls roughly exponentially until close to the Sun’s edge. It is safe to say that significantly far away from the Sun’s edge $A(x)$ is zero.

A particularly simple way of understanding the propagation of electron-type neutrinos produced in the Sun’s core to the Earth is to start with a ν_e state in the basis of the eigenstates of the Hamiltonian evaluated at the production point, $|\nu_e\rangle = \cos \vartheta_M(0) |\nu_L\rangle + \sin \vartheta_M(0) |\nu_H\rangle$, where $|\nu_H\rangle$ ($|\nu_L\rangle$) correspond to the highest (lowest) instantaneous Hamiltonian eigenstate. The matter mixing angle $\vartheta_M \equiv \vartheta_M(0)$ is given by

$$\cos 2\vartheta_M = \frac{\Delta m^2 \cos 2\vartheta - 2E_\nu A}{\sqrt{(\Delta m^2)^2 + A^2 - 4E_\nu A \Delta m^2 \cos 2\vartheta}}. \quad (2.9)$$

The evolution of this initial state from the Sun’s core is described by an arbitrary unitary matrix until the neutrino reaches the Sun’s edge. From this point on, one can rotate the state to the mass basis and follow the vacuum evolution of the state. Therefore, $P_{ee}(x)$, where x is the distance from the Sun’s edge to some point far away from the Sun (for example, the Earth), is

$$P_{ee}(x) = \left| \begin{pmatrix} U_{e1}^* & U_{e2}^* \end{pmatrix} \begin{pmatrix} 1 & 0 \\ 0 & e^{-i\frac{\Delta m^2 x}{2E_\nu}} \end{pmatrix} \begin{pmatrix} A & B \\ -B^* & A^* \end{pmatrix} \begin{pmatrix} \cos \vartheta_M \\ \sin \vartheta_M \end{pmatrix} \right|^2, \quad (2.10)$$

where overall phases in the amplitude have been neglected. The matrix parametrised by A, B represents the evolution of the system from the Sun's core to vacuum, and also rotates the state into the mass basis.[‡] Expanding Eq. (2.10), and assuming that there is no coherence in the Sun's core between ν_L and ν_H ,[§] one arrives at the well known expression (these have been first derived using a different language in [28] and [29])

$$P_{ee}(x) = P_1 \cos^2 \vartheta + P_2 \sin^2 \vartheta - \cos 2\vartheta_M \sqrt{P_c(1 - P_c)} \sin 2\vartheta \cos \left(\frac{\Delta m^2 x}{2E_\nu} + \delta \right), \quad (2.11)$$

where δ is the phase of AB^* , $P_c \equiv |B|^2 = 1 - |A|^2$ is the “level crossing probability”, and $P_1 = 1 - P_2 = \frac{1}{2} + \frac{1}{2}(1 - 2P_c) \cos 2\vartheta_M$ is interpreted as the probability that the neutrino exits the Sun as a ν_1 .

Eq. (2.11) should be valid in all cases of interest, and contains a large amount of features. In the case of the solar neutrino puzzle, the neutrino energies of interest range between hundreds of keV to ten MeV, and matter effects start to play a role for values of Δm^2 as high as 10^{-4} eV^2 . In the adiabatic limit ($P_c \rightarrow 0$) very small values of P_{ee} are attainable when $\cos 2\vartheta_M \rightarrow -1$ and $\sin^2 \vartheta$ is small. More generally, in this limit $P_{ee} = \sin^2 \vartheta$. This is what happens for all solar neutrino energies in the case of the LOW solution,[¶] for solar neutrino energies above a few MeV in the case of the LMA solution, and for 400 keV $\lesssim E_\nu \lesssim 1$ MeV energies in the case of the SMA solution. In the extremely nonadiabatic limit, which is reached when $\Delta m^2/2E_\nu \ll A$, $P_c \rightarrow \cos^2 \vartheta$ and $\cos 2\vartheta_M \rightarrow -1$, the original vacuum oscillation expression is obtained, up to the “matter phase” δ . This is generically what happens in the VAC solution to the solar neutrino puzzle.

If the electron number density is in fact exponential, one can solve Eq. (2.7) exactly [30, 31]. For $N_e(x) = N_e(0) e^{-x/r_0}$, where $x = 0$ is the centre of the Sun,

$$P_c = \frac{e^{-\gamma \sin^2 \vartheta} - e^{-\gamma}}{1 - e^{-\gamma}}, \quad (2.12)$$

[‡]The most general form of a 2×2 unitary matrix is $\begin{pmatrix} A & B \\ -B^* & A^* \end{pmatrix} \begin{pmatrix} 1 & 0 \\ 0 & e^{i\zeta} \end{pmatrix}$, where $|A|^2 + |B|^2 = 1$ and $0 \leq \zeta \leq 2\pi$. In the case of neutrino oscillations, however, the physical quantities are $|A|^2$ and the phase of AB^* , and therefore ζ can be ignored.

[§]This is in general the case, because one has to consider that neutrinos are produced at different points in space and time.

[¶]See [9, 10, 11] for the labelling of the regions of the parameter space that solve the solar neutrino puzzle

[31, 32] where

$$\gamma = 2\pi r_0 \frac{\Delta m^2}{2E_\nu} = 1.05 \left(\frac{\Delta m^2}{10^{-6} \text{ eV}^2} \right) \left(\frac{1 \text{ GeV}}{E_\nu} \right), \quad (2.13)$$

for $r_0 = R_\odot/10.54 = 6.60 \times 10^4 \text{ km}$ [27]. In the case of the Sun, the exponential profile approximation has been examined [32], and was shown to be very accurate, especially if one allows r_0 to vary as a function of $\Delta m^2/2E_\nu$.

The exact expression for δ has also been obtained [28], and the readers are referred to [33] for details concerning physical implications of the matter phase. Its effects will not be discussed here any further.

2.3 The Case of Antineutrinos

Antineutrinos that are produced in the Sun's core obey a differential equation similar to Eq. (2.7), except that the sign of the matter potential changes, *i.e.* $A(x) \leftrightarrow -A(x)$, and $U_{\alpha i} \leftrightarrow U_{\alpha i}^*$ (this is immaterial since, in the two-flavour mixing case, all $U_{\alpha i}$ are real).

Instead of working out the probability of an electron-type antineutrino being detected as an electron-type antineutrino $P_{\bar{e}\bar{e}}$ from scratch, there is a very simple way of relating it to P_{ee} . One only has to note that, if the following transformation is applied to Eq. (2.7): $\vartheta \rightarrow \pi/2 - \vartheta$, subtract the matrix $A(1_{2 \times 2})$, where $1_{2 \times 2}$ is the 2×2 identity matrix and relabel $\nu_e(x) \leftrightarrow \nu_x(x)$, the equation of motion for antineutrinos is obtained.^{||} Therefore, $P_{\bar{e}\bar{e}}(\vartheta) = P_{xx}(\pi/2 - \vartheta) = P_{ee}(\pi/2 - \vartheta)$ (this was pointed out in [34]). Remember that, in the case of vacuum oscillations, ϑ is physically equivalent to $\pi/2 - \vartheta$, so $P_{\bar{e}\bar{e}} = P_{ee}$. In the more general case of nontrivial matter effects, this is clearly not the case, since the presence of matter (or antimatter) explicitly breaks CP -invariance.

It is curious to note that, in the case of two-flavour oscillations, there is no T -noninvariance, *i.e.*, $P_{\alpha\beta} = P_{\beta\alpha}$, while there is potentially large CP violation, *i.e.*, $P_{\alpha\beta} \neq P_{\bar{\alpha}\bar{\beta}}$, even if the Hamiltonian for the system is explicitly T -noninvariant and CP -noninvariant, as is the case of the propagation of neutrinos produced in the Sun (namely $A(t)$ is a generic function of time and $A(t)$ for neutrinos is $-A(t)$ for antineutrinos).

^{||}If one decides to limit $0 \leq \vartheta \leq \pi/4$, a similar result can be obtained if $\Delta m^2 \rightarrow -\Delta m^2$, explicitly $P_{\bar{e}\bar{e}}(\Delta m^2) = P_{ee}(-\Delta m^2)$.

3 Three Flavour Oscillations

Currently, aside from the solar neutrino puzzle, there is an even more convincing evidence for neutrino oscillations, namely the suppression of the muon-type neutrino flux in atmospheric neutrino experiments [1]. This atmospheric neutrino puzzle is best solved by $\nu_\mu \leftrightarrow \nu_\tau$ oscillations with a large mixing angle [2]. Furthermore, the values of Δm^2 required to solve the atmospheric neutrino puzzle are at least one order of magnitude higher than the values required to solve the solar neutrino puzzle. For this reason, in order to solve both neutrino puzzles in terms of neutrino oscillations, three neutrino families are required.

In this section, the oscillations of three neutrino flavours will be considered. In order to simplify the discussion, I will concentrate on neutrinos with energies ranging from a few to tens of GeV, which is the energy range expected for neutrinos produced by the annihilation of dark matter particles which are possibly trapped inside the Sun. Furthermore, a number of experimentally inspired constraints on the neutrino oscillation parameter space will be imposed, as will become clear later.

3.1 Generalities

Similar to the two-flavour case, the “mapping” between the flavour eigenstates, ν_e , ν_μ and ν_τ and the mass eigenstates ν_i , $i = 1, 2, 3$ with masses m_i can be performed with a general 3×3 unitary matrix, which is parametrised by three mixing angles (θ , ω , and ξ) and a complex phase ϕ . In short hand notation $\nu_\alpha = U_{\alpha i} \nu_i$ where $\alpha = e, \mu, \tau$ and $i = 1, 2, 3$. The MNS mixing matrix [14] will be written, similar to the standard CKM quark mixing matrix [35], as

$$\begin{pmatrix} U_{e1} & U_{e2} & U_{e3} \\ U_{\mu1} & U_{\mu2} & U_{\mu3} \\ U_{\tau1} & U_{\tau2} & U_{\tau3} \end{pmatrix} = \begin{pmatrix} c\omega c\xi & s\omega c\xi & s\xi e^{i\phi} \\ -s\omega c\theta - c\omega s\theta s\xi e^{-i\phi} & c\omega c\theta - s\omega s\theta s\xi e^{-i\phi} & s\theta c\xi \\ s\omega s\theta - c\omega c\theta s\xi e^{-i\phi} & -c\omega s\theta - s\omega c\theta s\xi e^{-i\phi} & c\theta c\xi \end{pmatrix}, \quad (3.1)$$

where $c\zeta \equiv \cos \zeta$ and $s\zeta \equiv \sin \zeta$ for $\zeta = \omega, \theta, \xi$. If the neutrinos are Majorana particles, two extra phases should be added to the MNS matrix, but, since they play no role in the physics of neutrino oscillations, they can be safely ignored. All physically distinguishable situations can be obtained if one allows $0 \leq \phi \leq \pi$, all angles to vary between 0 and $\pi/2$ and no restriction is imposed on the sign of the mass-squared differences, $\Delta m_{ij}^2 \equiv m_i^2 - m_j^2$.

Note that there are only two independent mass-squared differences, which are chosen here to be Δm_{21}^2 and Δm_{31}^2 .

All experimental evidence from solar, atmospheric, and reactor neutrino experiments [1, 3, 4, 5, 6, 7, 36] can be satisfied,* somewhat conservatively, by assuming [26]: $10^{-4} \text{ eV}^2 \lesssim |\Delta m_{31}^2| \simeq |\Delta m_{32}^2| \lesssim 10^{-2} \text{ eV}^2$, $0.3 \lesssim \sin^2 \theta \lesssim 0.7$, $10^{-11} \text{ eV}^2 \lesssim |\Delta m_{21}^2| \lesssim 10^{-4} \text{ eV}^2$, $\sin^2 \xi \lesssim 0.1$, while ω is mostly unconstrained. There is presently no information on ϕ . In determining these bounds, it was explicitly assumed that only three active neutrinos exist.

A few comments about the constraints imposed above are in order. First, one may complain that ω is more constrained than mentioned above by the solar neutrino data. The situation is far from definitive, however. As pointed out recently in [11] if the uncertainty on the ^8B neutrino flux is inflated or if some of the experimental data is not considered (especially the Homestake data [3]) in the fit, a much larger range of Δm_{21}^2 and ω is allowed. Furthermore, if three-flavour mixing is considered [12], different regions in the parameter space Δm_{21}^2 - $\sin^2 \omega$ are allowed for different values of $\sin^2 \xi$, even if $\sin^2 \xi$ is constrained to be small.

Second, the limit from the Chooz and Palo Verde reactor experiments [36] do not constrain $\sin^2 \xi$ for $|\Delta m_{31}^2| \lesssim 10^{-3} \text{ eV}^2$. Furthermore, their constraints are to $\sin^2 2\xi$, so values of $\sin^2 \xi$ close to one should also be allowed. However, the constraints from the atmospheric neutrino data require $\cos^2 \xi$ to be close to one. This is easy to understand. Assuming that L_{21}^{osc} is much larger than the Earth's diameter and that $\Delta m_{31}^2 = \Delta m_{32}^2$,

$$P_{\mu\mu}^{\text{atm}} = 1 - 4 \cos^2 \xi \sin^2 \theta (1 - \cos^2 \xi \sin^2 \theta) \sin^2 \left(\frac{\Delta m_{31}^2 x}{4E_\nu} \right), \quad (3.2)$$

according to upcoming Eq. (3.3). Almost maximal mixing implies that $\cos^2 \xi \sin^2 \theta \simeq 1/2$. With the further constraint from P_{ee}^{atm} , namely $\sin^2 2\xi \simeq 0$, one concludes that $\cos^2 \xi \simeq 1$ and $\sin^2 \theta \simeq 1/2$.

In the case of oscillations in vacuum, it is straight forward to compute the oscillation probabilities $P_{\alpha\beta}$ of detecting a flavour β given that a flavour α was produced.

$$P_{\alpha\beta} = \sum_{i,j} U_{\alpha i}^* U_{\alpha j} U_{\beta i} U_{\beta j}^* e^{i \frac{\Delta m_{ij}^2 x}{2E_\nu}} \quad (3.3)$$

*There is evidence for neutrino oscillations coming from the LSND experiment [37]. Such evidence has not yet been confirmed by another experiment, and will not be considered in this paper. If, however, it is indeed confirmed, it is quite likely that a fourth, sterile, neutrino will have to be introduced into the picture.

The three different oscillation lengths, L_{osc}^{ij} , are numerically given by

$$L_{\text{osc}}^{ij} = \frac{4\pi E_\nu}{\Delta m_{ij}^2} = 2.47 \times 10^8 \text{km} \left(\frac{E}{1 \text{ GeV}} \right) \left(\frac{10^{-8} \text{ eV}^2}{\Delta m_{ij}^2} \right), \quad (3.4)$$

which are to be compared to the Earth-Sun distance ($1 \text{ a.u.} = 1.496 \times 10^8 \text{ km}$). In the energy range of interest, $1 \text{ GeV} \lesssim E_\nu \lesssim 100 \text{ GeV}$ and given the experimental constraints on the parameter space described above, it is easy to see that L_{osc}^{31} and L_{osc}^{32} are much smaller than 1 a.u. , and that its effects should “wash out” due to any realistic neutrino energy spectrum, detector energy resolution, or other “physical” effects. Such terms will therefore be neglected henceforth. In contrast, L_{osc}^{21} maybe as large as (and maybe even much larger than!) the Earth-Sun distance. Note that a nonzero phase ϕ implies T -violation, *i.e.*, $P_{\alpha\beta} \neq P_{\beta\alpha}$, unless $L_{\text{osc}}^{21} \gg 1 \text{ a.u.}$. This will be discussed in more detail later.

In the presence of neutrino-medium interactions, the situation is, in general, more complicated (indeed, much more!). Similar to the two-neutrino case, it is important to discuss what is known about the oscillation probabilities. From the conservation of probability one has

$$\begin{aligned} P_{ee} + P_{e\mu} + P_{e\tau} &= 1, \\ P_{\mu e} + P_{\mu\mu} + P_{\mu\tau} &= 1, \\ P_{\tau e} + P_{\tau\mu} + P_{\tau\tau} &= 1, \end{aligned} \quad (3.5)$$

and, similar to the two-neutrino case, unitarity of the Hamiltonian evolution implies

$$\begin{aligned} P_{ee} + P_{\mu e} + P_{\tau e} &= 1, \\ P_{e\mu} + P_{\mu\mu} + P_{\tau\mu} &= 1, \end{aligned} \quad (3.6)$$

A third equation of this kind, $P_{e\tau} + P_{\mu\tau} + P_{\tau\tau} = 1$, is redundant. As before, Eqs. (3.6) can be understood by arguing that, if equal numbers of all neutrino species are produced, the number of ν_β 's to be detected should be the same, regardless of β , simply because the neutrino propagation is governed by a unitary operator.

One may therefore express all $P_{\alpha\beta}$ in terms of only four quantities. Here, these are chosen to be P_{ee} , $P_{e\mu}$, $P_{\mu\mu}$, and $P_{\tau\tau}$. The others are given by

$$P_{e\tau} = 1 - P_{ee} - P_{e\mu},$$

$$\begin{aligned}
P_{\mu e} &= 1 + P_{\tau\tau} - P_{ee} - P_{\mu\mu} - P_{e\mu}, \\
P_{\mu\tau} &= P_{ee} + P_{e\mu} - P_{\tau\tau}, \\
P_{\tau e} &= P_{\mu\mu} + P_{e\mu} - P_{\tau\tau}, \\
P_{\tau\mu} &= 1 - P_{\mu\mu} - P_{e\mu}.
\end{aligned} \tag{3.7}$$

Note that, in general, $P_{\alpha\beta} \neq P_{\beta\alpha}$.

3.2 Oscillation of Neutrinos Produced in the Sun's Core

The propagation of neutrinos in the Sun's core can, similar to the two-neutrino case, be described by the differential equation

$$\frac{d}{dx}\nu_\alpha(r) = -i \left(\sum_{i=2}^3 \left(\frac{\Delta m_{i1}^2}{2E_\nu} \right) U_{\alpha i}^* U_{\beta i} + A(x) \delta_{\alpha e} \delta_{\beta e} \right) \nu_\beta(r), \tag{3.8}$$

where $\delta_{\eta\zeta}$ is the Kronecker delta symbol. Terms proportional to the identity $\delta_{\alpha\beta}$ are neglected because they play no role in the physics of neutrino oscillations. The matter induced potential $A(x)$ is given by Eq.(2.8).

As in the two-neutrino case, it is useful to first discuss the initial states ν_α in the Sun's core, and to express them in the basis of instantaneous Hamiltonian eigenstates, which will be referred to as $|\nu_H\rangle$, $|\nu_M\rangle$, and $|\nu_L\rangle$ (H = high, M = medium, and L = low). Therefore

$$|\nu_\alpha\rangle = H_\alpha |\nu_H\rangle + M_\alpha |\nu_M\rangle + L_\alpha |\nu_L\rangle, \tag{3.9}$$

where $\langle \nu_\alpha | \nu_{\alpha'} \rangle = \delta_{\alpha\alpha'}$. As before (see Eq. 2.10), the probability of detecting this initial state as a β -type neutrino far away from the Sun (*e.g.*, at the Earth) is given by

$$P_{\alpha\beta} = \left| \begin{pmatrix} U_{\beta 1}^* & U_{\beta 2}^* & U_{\beta 3}^* \end{pmatrix} \begin{pmatrix} 1 & 0 & 0 \\ 0 & e^{-i\frac{\Delta m_{21}^2 x}{2E_\nu}} & 0 \\ 0 & 0 & e^{-i\frac{\Delta m_{31}^2 x}{2E_\nu}} \end{pmatrix} (V_{3\times 3}) \begin{pmatrix} L_\alpha \\ M_\alpha \\ H_\alpha \end{pmatrix} \right|^2, \tag{3.10}$$

where $V_{3\times 3}$ is an arbitrary 3×3 unitary matrix which takes care of propagating the initial state until the edge of the Sun and rotating the state into the mass basis.

In order to proceed, it is useful take advantage of the constraints on the neutrino parameter space and the energy range of interest. Note that

$A \gtrsim \frac{|\Delta m_{31}^2|}{2E_\nu} \gg \frac{|\Delta m_{21}^2|}{2E_\nu}$ (remember that the energy range of interest is $1 \text{ GeV} \lesssim E_\nu \lesssim 100 \text{ GeV}$ and that $A \simeq 6 \times 10^{-3} \text{ eV}^2/\text{GeV}$). It has been shown explicitly [17], assuming the neutrino mass-squared hierarchy to be $m_3^2 > m_2^2 > m_1^2$,[†] that, if the mass-squared differences are very hierarchical ($|\Delta m_{31}^2| \gg |\Delta m_{21}^2|$), the three-level system “decouples” into two two-level systems, *i.e.*, one can first deal with matter effects in the “ $H - M$ ” system and then with the matter effects in the “ $M - L$ ” system. One way of understanding why this is the case is to realize that the “resonance point” corresponding to the Δm_{31}^2 is very far away from the resonance point corresponding to Δm_{21}^2 . With this in mind, it is fair to approximate (this is similar to what is done, for example, in [38])

$$V_{3 \times 3} = \begin{pmatrix} A^L & B^L & 0 \\ -B^{L*} & A^{L*} & 0 \\ 0 & 0 & 1 \end{pmatrix} \begin{pmatrix} 1 & 0 & 0 \\ 0 & A^H & B^H \\ 0 & -B^{H*} & A^{H*} \end{pmatrix}, \quad (3.11)$$

where $|B^H|^2 = 1 - |A^H|^2 \equiv P_c^H$, $|B^L|^2 = 1 - |A^L|^2 \equiv P_c^L$. The superscripts H, L correspond to the “high” and the “low” resonances, respectively.

It is also possible to obtain an approximate expression for the initial states in the Sun’s core. Following the result outline above, this state should be described by two matter angles, ξ_M and ω_M , corresponding to each of the two-level systems. Both should be given by Eq. (2.9), where, in the case of $\cos 2\xi_M$, ϑ is to be replaced by ξ and Δm^2 by Δm_{31}^2 , while in the case of $\cos 2\omega_M$, ϑ is to be replaced by ω , Δm^2 by Δm_{21}^2 and A is to be replaced by $A \cos \xi$ [38, 12]. Furthermore, because $A \cos \xi \gg \frac{|\Delta m_{21}^2|}{2E_\nu}$, $\cos 2\omega_M$ can be safely replaced by -1 (remember that $\cos^2 \xi \gtrsim 0.9$). Within these approximations, in the Sun’s core,

$$\begin{aligned} |\nu_e\rangle &= \sin \xi_M |\nu_H\rangle + \cos \xi_M |\nu_M\rangle, \\ |\nu_\mu\rangle &= \sin \theta \cos \xi_M |\nu_H\rangle - \sin \theta \sin \xi_M |\nu_M\rangle - \cos \theta |\nu_L\rangle, \\ |\nu_\tau\rangle &= \cos \theta \cos \xi_M |\nu_H\rangle - \cos \theta \sin \xi_M |\nu_M\rangle + \sin \theta |\nu_L\rangle. \end{aligned} \quad (3.12)$$

The accuracy of this approximation has been tested numerically in the range of parameters of interest, and the difference between the “exact” result and the approximate result presented in Eq. (3.12) is negligible.

Keeping all this in mind, it is straight forward to compute all oscillation probabilities, starting from Eq. (3.10). From here on, $\phi = 0$ (no T -violating phase in the mixing matrix, such that all $U_{\alpha i}$ are real) will be assumed, in

[†]I will work under this assumption for the time being.

order to simplify expressions and render the results cleaner. In the end of the day one obtains

$$P_{\alpha\beta} = a_\alpha^2(U_{\beta 1})^2 + b_\alpha^2(U_{\beta 2})^2 + c_\alpha^2(U_{\beta 3})^2 + 2a_\alpha b_\alpha(U_{\beta 1}U_{\beta 2}) \cos\left(\frac{\Delta m_{21}^2 x}{2E_\nu} + \delta^L\right) \quad (3.13)$$

or

$$P_{\alpha\beta} = (a_\alpha U_{\beta 1} + b_\alpha U_{\beta 2})^2 + c_\alpha^2(U_{\beta 3})^2 - 4a_\alpha b_\alpha(U_{\beta 1}U_{\beta 2}) \sin^2\left(\frac{\Delta m_{21}^2 x}{4E_\nu} + \delta^L\right),$$

where δ^L is the matter phase, induced in the low resonance, and

$$\begin{aligned} a_e &= \sqrt{P_2^H P_c^L}, \\ b_e &= \sqrt{P_2^H(1 - P_c^L)}, \\ c_e &= \sqrt{P_3^H}, \\ a_\mu &= -\sqrt{(1 - P_c^L)} \cos \theta - \sqrt{P_3^H P_c^L} \sin \theta, \\ b_\mu &= \sqrt{P_c^L} \cos \theta - \sqrt{P_3^H(1 - P_c^L)} \sin \theta, \\ c_\mu &= \sqrt{P_2^H \sin^2 \theta}, \\ a_\tau &= \sqrt{(1 - P_c^L)} \sin \theta - \sqrt{P_3^H P_c^L} \cos \theta, \\ b_\tau &= -\sqrt{P_c^L} \sin \theta - \sqrt{P_3^H(1 - P_c^L)} \cos \theta, \\ c_\tau &= \sqrt{P_2^H \cos^2 \theta}, \end{aligned} \quad (3.14)$$

and $P_2^H = 1 - P_3^H = (|A^H|^2 \cos^2 \xi_M + |B^H|^2 \sin^2 \xi_M)$, which can also be written as $P_2^H = \frac{1}{2} + \frac{1}{2} (1 - 2P_c^H) \cos 2\xi_M$. This is to be compared with the expression for P_1 obtained in the two-flavour case. Note that $a_\alpha^2 + b_\alpha^2 + c_\alpha^2 = 1$. The effect of δ^L will not be discussed here and from here on δ^L will be set to zero. For details about the significance of δ^L for solar neutrinos in the two-flavour case, readers are referred to [28, 33].

Many comments are in order. First, in the nonadiabatic limit which can be obtained for very large energies, $P_c^H \rightarrow \cos^2 \xi$, $P_c^L \rightarrow \cos^2 \omega$ and $\cos 2\xi_M \rightarrow -1$. It is trivial to check that in this limit $a_\alpha \rightarrow U_{\alpha 1}$, $b_\alpha \rightarrow U_{\alpha 2}$, $c_\alpha \rightarrow U_{\alpha 3}$, and the vacuum oscillation result is reproduced, up to the matter induced phase δ^L .

Second, P_{ee} can be written as

$$P_{ee} = P_2^H \cos^2 \xi (P_{ee}^{2\nu}) + P_3^H \sin^2 \xi, \quad (3.15)$$

where $P_{ee}^{2\nu}$ is the two-neutrino result obtained in the previous section (see Eq. (2.11)) in the limit $\cos 2\vartheta_M \rightarrow -1$. It is easy to check that Eq. (2.11) would be exactly reproduced (with ϑ_M replaced by ω_M , of course) if the $\cos 2\omega_M = -1$ approximation were dropped.

For solar neutrino energies ($100 \text{ keV} \lesssim E_\nu \lesssim 10 \text{ MeV}$), $\xi_M \rightarrow \xi$, $P_c^H \rightarrow 0$ and therefore P_2^H (P_3^H) $\rightarrow \cos^2 \xi$ ($\sin^2 \xi$), reproducing correctly the result of the survival probability of electron-type solar neutrinos in a three-flavour oscillation scenario (see [26] and references therein). In this scenario there is no “ $H - L$ ” resonance inside the Sun, because $\frac{|\Delta m_{31}^2|}{2E_\nu} \gg A$ for solar neutrino energies.

On the other hand, in the case $P_c^H \rightarrow 0$ and $\cos 2\xi_M \rightarrow -1$, $P_3^H \rightarrow 1$ and electron-type neutrinos exit the Sun as a pure ν_3 mass eigenstate, and do not undergo vacuum oscillations even if Δm_{21}^2 is very small. In contrast, ν_μ and ν_τ always undergo vacuum oscillations if Δm_{21}^2 is small enough. The reason for this is simple. The generic feature of matter effects is to “push” ν_e into the heavy mass eigenstate, while ν_μ and ν_τ are “pushed” into the light mass eigenstates. This situation is changed by nonadiabatic effects, as argued above.

Finally, it is important to note that all equations obtained are also valid in the case of inverted hierarchies ($m_3^2 < m_{1,2}^2$ or $m_2^2 < m_1^2$). This has been discussed in detail in the two-neutrino oscillation case [39], and is also applicable here. It is worthwhile to point out that, in the approximation $\Delta m_{31}^2 \simeq \Delta m_{32}^2$ the transformation $\Delta m_{21}^2 \rightarrow -\Delta m_{21}^2$ can be reproduced by transforming $\omega \rightarrow \pi/2 - \omega$, $\theta \rightarrow \pi - \theta$ and redefining the sign of ν_τ . Therefore, one is in principle allowed to fix the sign of Δm_{21}^2 as long as θ is allowed to vary between 0 and π .

In the case of inverted hierarchies (especially when $\Delta m_{31}^2 < 0$) one expects to see no “level crossing” (indeed, matter effects tend to increase the distance between the “energy” levels in this case), but matter effects are still present, because the initial state in the Sun’s core can be nontrivial (i.e., $\vartheta_M \neq \vartheta$). Note that ν_e is still “pushed” towards ν_H , even in the case of inverted hierarchies, and the expressions for the matter mixing angles Eq. (2.9), and the initial states inside the Sun Eq. (3.12) are still valid. The consequence of no “level crossing” is that the adiabatic limit does not connect, for example, $\nu_H \rightarrow \nu_3$ but $\nu_H \rightarrow \nu_2$ (or ν_1 , depending on the sign of Δm_{21}^2). This information is in fact contained in the equations above. The crucial feature is that, for example, when $\Delta m_{31}^2 < 0$, $P_c^H \rightarrow 1$ in the “adiabatic limit,”

and the matrix $V_{3 \times 3}$ correctly “connects” $\nu_H \rightarrow \nu_2$ (or ν_1)! Another curious feature is that, in the limit $|\Delta m_{31}^2|/2E_\nu \gg A$, $\cos 2\xi_M \rightarrow -\cos 2\xi$, $P_c^H \rightarrow 1$ and Eq. (3.15) correctly reproduces the survival probability of electron-type solar neutrinos in the three-flavour oscillation case. Note that on this case the sign of Δm_{31}^2 does not play any role, as expected. On the other hand, it is still true that $P_c^{(H,L)} \rightarrow \cos^2(\xi, \omega)$ in the extreme nonadiabatic limit, and vacuum oscillation results are reproduced, as expected. Again, in this limit, one is not sensitive to the sign of Δm_{31}^2 , as expected.

3.3 The Case of Antineutrinos

As in the two-neutrino case, the difference between neutrinos and antineutrinos is that the equivalent of Eq. (3.8) for antineutrinos can be obtained by changing $A(x) \rightarrow -A(x)$ and $U_{\alpha i} \leftrightarrow U_{\alpha i}^*$. Unlike the two-flavour case, however, there is no set of variable transformations that allows one to exactly relate the differential equation for the neutrino and antineutrino systems. One should, however, note that if the signs of both Δm^2 are changed and $U_{\alpha i} \leftrightarrow U_{\alpha i}^*$, the neutrino equation turns into the antineutrino equation, up to an overall sign. This means, for example, that the instantaneous eigenvalues of the antineutrino Hamiltonian can be read from the eigenvalues of the neutrino Hamiltonian with $\Delta m_{ij}^2 \leftrightarrow -\Delta m_{ij}^2$, $U_{\alpha i} \leftrightarrow U_{\alpha i}^*$ plus an overall sign.

When it comes to computing $P_{\bar{\alpha}\bar{\beta}}$ this global sign difference is not relevant, and therefore $P_{\bar{\alpha}\bar{\beta}}(\Delta m_{ij}^2, U_{\alpha i}) = P_{\alpha\beta}(-\Delta m_{ij}^2, U_{\alpha i}^*)$.

4 Results and Discussions

This section contains the compilation and discussion of a number of results concerning the oscillation of GeV neutrinos of all species produced in the Sun’s core. The goal here is to explore the multidimensional parameter space spanned by Δm_{21}^2 , Δm_{31}^2 , $\sin^2 \omega$, $\sin^2 \theta$, and $\sin^2 \xi$ (and E_ν).

It will be assumed throughout that the electron number density profile of the Sun is exponential, so that Eq. (2.12) can be used. As mentioned before, the numerical accuracy of this approximation is quite good, and certainly good enough for the purposes of this paper. Therefore, both P_c^H and P_c^L which appear in Eq. (3.13) will be given by Eqs. (2.12, 2.13), with $\vartheta \rightarrow \xi$, $\Delta m^2 \rightarrow \Delta m_{31}^2$ in the former, and $\vartheta \rightarrow \omega$, $\Delta m^2 \rightarrow \Delta m_{21}^2$ in the latter.

When computing $P_{\alpha\beta}$, an averaging over “seasons” is performed, which

“washes out” the effect of very small oscillation wavelengths. Furthermore, integration over neutrino energy distributions is performed. Finally, all $P_{\alpha\beta}$ to be computed should be understood as the value of $P_{\alpha\beta}$ in the Earth’s surface, *i.e.*, Earth matter effects are not included. This is done in order to make the Sun matter effects in the evaluation of $P_{\alpha\beta}$ more clear. It should be stressed that Earth matter effects may play a significant role for particular regions of the parameter space, but the discussion of such effects will be left for another opportunity.

Because the parameter space to be explored is multidimensional, it is necessary to make two-dimensional projections of it, such that “illustrative” points are required. The following points in the parameter space are chosen, all inspired by the current experimental situation:

- ATM: $\Delta m_{31}^2 = 3 \times 10^{-3} \text{ eV}^2$, $\sin^2 \theta = 0.5$, and $\sin^2 \xi = 0.01$,
- LMA: $\Delta m_{21}^2 = 2 \times 10^{-5} \text{ eV}^2$, $\sin^2 \omega = 0.2$,
- SMA: $\Delta m_{21}^2 = 6 \times 10^{-6} \text{ eV}^2$, $\sin^2 \omega = 0.001$,
- LOW: $\Delta m_{21}^2 = 1 \times 10^{-7} \text{ eV}^2$, $\sin^2 \omega = 0.4$,
- VAC: $\Delta m_{21}^2 = 1 \times 10^{-10} \text{ eV}^2$, $\sin^2 \omega = 0.55$.

ATM corresponds to the best fit point of the solution to the atmospheric neutrino puzzle [2], and a value of $\sin^2 \xi = 0.01$ which is consistent with all the experimental bounds. Note that some “subset” of ATM will always be assumed (for example, $\sin^2 \theta$ is fixed while exploring the $(\Delta m_{31}^2 \times \sin^2 \xi)$ -plane). For each analysis, it will be clear what are the “variables” and what quantities are held fixed at their “preferred point” values. All other points refer to sample points in the regions which best solve the solar neutrino puzzle [9, 10, 11], and the notation should be obvious. Initially a flat neutrino energy distribution with $E_\nu^{min} = 1 \text{ GeV}$ and $E_\nu^{max} = 5 \text{ GeV}$ is considered (for concreteness), and the case of higher average energies is briefly discussed later.

4.1 The Case of Vacuum Oscillations

If neutrinos were produced and propagated exclusively in vacuum, the oscillation probabilities would be given by Eq. (3.3). This would be the case of

neutrinos produced in the Sun's core if either the electron number density were much smaller than its real value or if very low energy neutrinos were being considered. Nonetheless, it is still useful to digress some on the “would be” vacuum oscillation probabilities in order to understand better the matter effects.

In the case of pure vacuum oscillations, it is trivial to check that $P_{\alpha\beta} = P_{\beta\alpha}$ (remember that the MNS matrix phase ϕ has been set to zero), and therefore all $P_{\alpha\beta}$ can be parametrised by three quantities, namely $P_{\alpha\alpha}$, $\alpha = e, \mu, \tau$. It is easy to show that

$$P_{\alpha\beta} = P_{\beta\alpha} \Leftrightarrow P_{e\mu} = \frac{1}{2}(1 + P_{\tau\tau} - P_{\mu\mu} - P_{ee}). \quad (4.1)$$

From Eq. (3.3)

$$\begin{aligned} P_{\alpha\alpha} &= U_{\alpha 1}^4 + U_{\alpha 2}^4 + U_{\alpha 3}^4 + 2U_{\alpha 1}^2 U_{\alpha 2}^2 \cos\left(\frac{\Delta m_{21}^2 x}{2E_\nu}\right) \\ &\text{or} \\ P_{\alpha\alpha} &= (1 - U_{\alpha 3}^2)^2 + U_{\alpha 3}^4 - 4U_{\alpha 1}^2 U_{\alpha 2}^2 \sin^2\left(\frac{\Delta m_{21}^2 x}{4E_\nu}\right). \end{aligned} \quad (4.2)$$

Note that there is no dependency on Δm_{31}^2 . Particularly simple limits can be reached when L_{osc}^{21} is either very small or very large compared with the Earth-Sun distance. In both limits $P_{\alpha\alpha}$ is independent of Δm_{21}^2 and, in the latter case, $P_{\alpha\alpha}$ depends only on $U_{\alpha 3}^2$. Fig. 1 depicts constant $P_{\alpha\beta}$ contours in the $(\Delta m_{21}^2 \times \sin^2 \omega)$ -plane, at ATM. Remember that, here, $P_{e\mu}$ is not an independent quantity but is a linear combination of all $P_{\alpha\alpha}$. Note that P_{ee} is symmetric for $\omega \rightarrow \pi/2 - \omega$, and that $P_{\mu\mu} \leftrightarrow P_{\tau\tau}$ when $\omega \rightarrow \pi/2 - \omega$. The latter property is a consequence of $\theta = \pi/4$. Also, in the case of P_{ee} , the $L_{\text{osc}}^{21} \rightarrow \infty$ coincides with the $\omega \rightarrow 0, \pi/2$ limit for any L_{osc}^{21} (this is because either U_{e1} or U_{e2} go to zero). This is not true of $P_{\mu\mu}$ or $P_{\tau\tau}$ unless $\sin^2 \xi = 0$. Another important consequence of $L_{\text{osc}}^{21} \gg 1$ a.u. is that T -violating effects are absent, even if ϕ is nonzero. This can be seen by looking at the second expression in Eq. (4.2), which is a function only of $|U_{\alpha 3}|^2$ in the limit $L_{\text{osc}}^{21} \rightarrow \infty$.

Finally, one should note that oscillatory effects are maximal for $\Delta m_{21}^2 \simeq 2 \times 10^{-8} \text{ eV}^2$. In this region $\cos\left(\frac{\Delta m_{21}^2 x}{2E_\nu}\right) \simeq -1$, and the largest suppression to all $P_{\alpha\alpha}$ is obtained when $U_{\alpha 1}^2 U_{\alpha 2}^2$ is maximum. For example, P_{ee} is smallest when $\omega = \pi/4$, since $U_{e1}^2 U_{e2}^2 \propto \sin^2 2\omega$. There are no “localised” maxima for $P_{\alpha\alpha}$ because $U_{\alpha 1}^2 U_{\alpha 2}^2$ is positive definite.

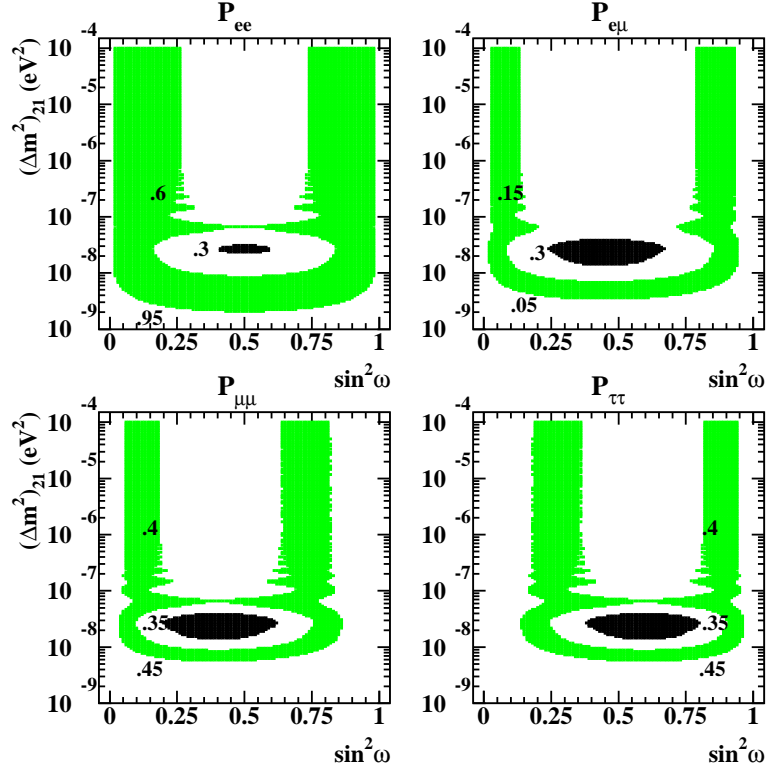


Figure 1: Constant $P_{\alpha\beta}$ contours in the $(\Delta m_{21}^2 \times \sin^2 \omega)$ -plane, at ATM (see text), in the case of pure vacuum oscillations.

4.2 “Normal” Neutrino Hierarchy

When matter effects are “turned on,” the situation can be dramatically different. This is especially true in the case of normal neutrino mass hierarchies ($m_1^2 < m_2^2 < m_3^2$), which will be discussed first.

The first effect one should observe is that, even though $L_{\text{osc}}^{31} \ll 1$ a.u., $P_{\alpha\beta}$ depend rather nontrivially on Δm_{31}^2 . This dependency comes from the terms P_3^H and $P_2^H = 1 - P_3^H$ in Eq. (3.13). Remember that P_3^H is interpreted as the probability that a ν_e produced in the Sun’s core exits the Sun as a ν_3 mass eigenstate. When matter effects are negligible (such as in the limit of small neutrino energies) $P_3^H \rightarrow \sin^2 \xi$, its “vacuum limit.” Fig. 2 depicts constant P_3^H contours in the $(\Delta m_{31}^2/E_\nu \times \sin^2 \xi)$ -plane.

Note that, for $\Delta m_{31}^2/E_\nu \sim 10^{-2}$ eV²/GeV, $P_3^H \rightarrow 1$, even for small values of $\sin^2 \xi$. In this region, ν_e ’s produced in the Sun’s core exit the Sun as pure

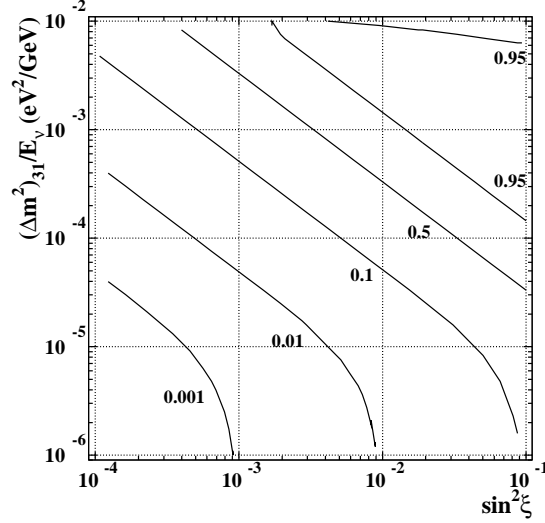


Figure 2: Contours of constant P_3^H (see text) in the $(\Delta m_{31}^2/E_\nu \times \sin^2 \xi)$ -plane.

ν_3 's. Therefore, $P_{e\alpha} \simeq U_{\alpha 3}^2$. Because of unitarity in the propagation, ν_μ 's and ν_τ 's exit the Sun as linear combinations of the light mass eigenstates, and may not only undergo vacuum oscillations but are also susceptible to further matter effects (dictated by the “ $M - L$ ” system, as described in Sec. 3). For future reference, at ATM, $P_3^H \simeq 0.87$ when averaged over the energy range mentioned in the beginning of this section.

As $\Delta m_{31}^2/E_\nu$ decreases (as is the case for higher energy neutrinos) the nonadiabaticity of the “ $H - M$ ” system starts to become relevant, and $P_3^H \rightarrow \sin^2 \xi$, as argued in Sec. 3.2. A hint of this behaviour can already be seen in Fig. 2, for small values of $\Delta m_{31}^2/E_\nu$.

The information due to the “ $M - L$ ” matter effect is encoded in P_c^L , present in Eq. (3.13). Fig. 3 depicts contours of constant $1 - P_c^L$ in the $(\Delta m_{21}^2/E_\nu \times \sin^2 \omega)$ -plane. One should note that $1 - P_c^L$ reaches its extreme nonadiabatic limit, $\sin^2 \omega$, when $\Delta m_{21}^2/E_\nu \lesssim 10^{-7} \text{ eV}^2/\text{GeV}$. For $\Delta m_{21}^2/E_\nu \gtrsim 10^{-7} \text{ eV}^2/\text{GeV}$, matter effects increase the value of $1 - P_c^L$.

One can use the intuition from the two-flavour solution to the solar neutrino puzzle to better appreciate the results presented here. In the case of the solutions to the solar neutrino puzzle, the energies of interest range from 100 keV to 10 MeV, and large matter effects happen around $\Delta m^2 \sim 10^{-5} \text{ eV}^2$. Furthermore, at $\Delta m^2 \sim 10^{-10} \text{ eV}^2$ one encounters the “just-so” solution, which is characterised by very long wave-length vacuum oscillations. Rescal-

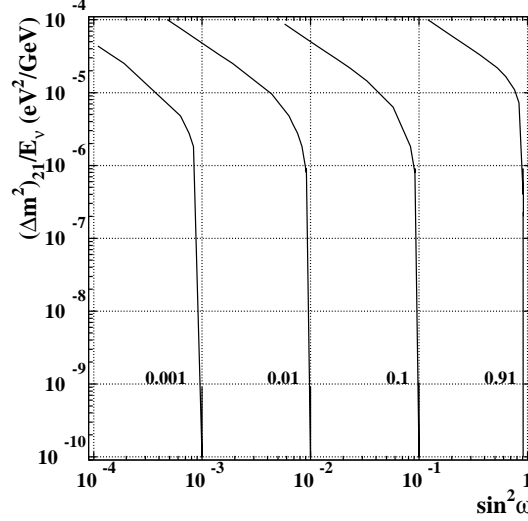


Figure 3: Contours of constant $1 - P_c^L$ (see text) in the $(\Delta m_{21}^2/E_\nu \times \sin^2 \omega)$ -plane.

ing to $O(\text{GeV})$ energies, the equivalent of the “just-so” solution happens for $\Delta m_{21}^2 \sim (10^{-8} - 10^{-7}) \text{ eV}^2$, while large matter effects would be present at $\Delta m^2 \sim (10^{-3} - 10^{-2}) \text{ eV}^2$. Indeed, one observes large matter effects for $\Delta m_{31}^2 \sim (10^{-3} - 10^{-2}) \text{ eV}^2$. $\Delta m_{21}^2 \sim (10^{-5} - 10^{-6}) \text{ eV}^2$ corresponds to the region between the LOW and VAC solutions, where matter effects distort $P_{\alpha\beta}$ from its pure vacuum value, but no dramatic suppression or enhancement takes place. Incidentally, this behaviour has physical consequences in the solution to the solar neutrino problem, as was first pointed out in [40].

Figs. 4 and 5 depict contours of constant $P_{\alpha\alpha}$ and $P_{e\mu}$ in the $(\Delta m_{31}^2 \times \sin^2 \xi)$ -plane. As expected, in the region where $P_3^H \sim 1$, P_{ee} and $P_{e\mu}$ do not depend on Δm_{21}^2 or $\sin^2 \omega$, namely $P_{ee} \sim \sin^2 \xi$ and $P_{e\mu} \sim 0.5 \cos^2 \xi$. Remember that the results depicted in Figs. 4 and 5 (and all other plots from here on) are for an energy band from 1 to 5 GeV. On the other hand, $P_{\mu\mu}$ and $P_{\tau\tau}$ do depend on the point (LMA, SMA, etc), even for $P_3^H \sim 1$, as foreseen. This dependence will be discussed in what follows.

In the limit $P_3^H = 1$, $\sin^2 \theta = 0.5$

$$c_\mu^2 = c_\tau^2 = 0, \quad (4.3)$$

$$a_\mu^2 = b_\tau^2 = 0.5(1 + 2\sqrt{P_c^L(1 - P_c^L)}), \quad (4.4)$$

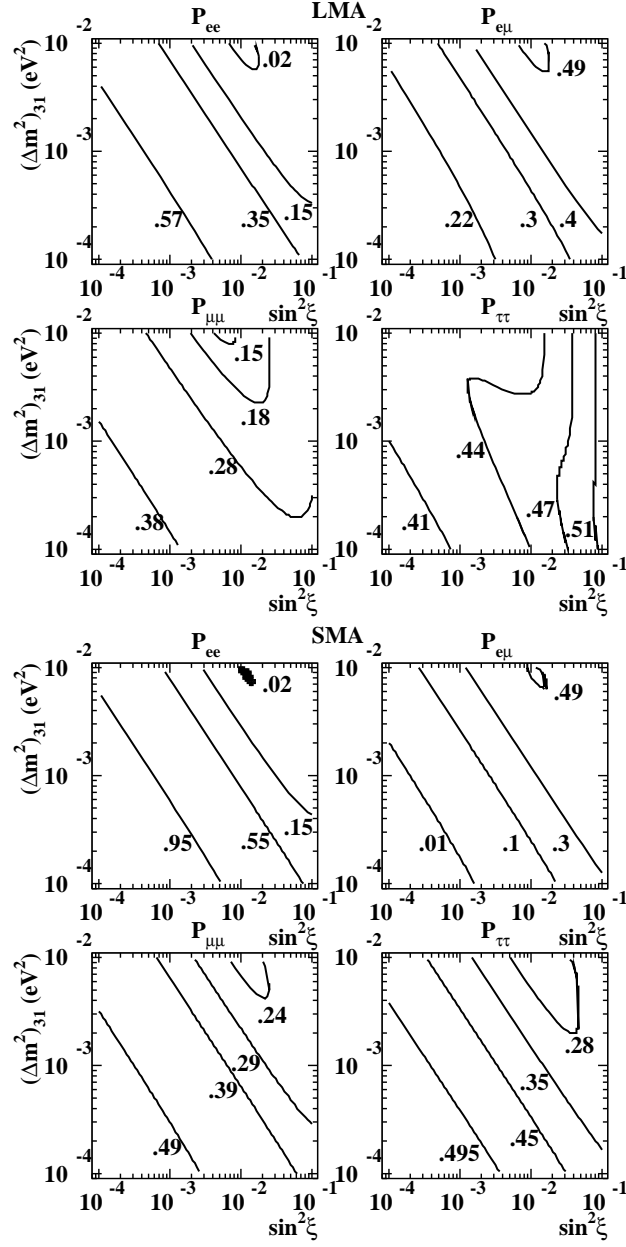


Figure 4: Constant $P_{\alpha\beta}$ contours in the $(\Delta m_{31}^2 \times \sin^2 \xi)$ -plane, at LMA (top) and SMA (bottom) (see text).

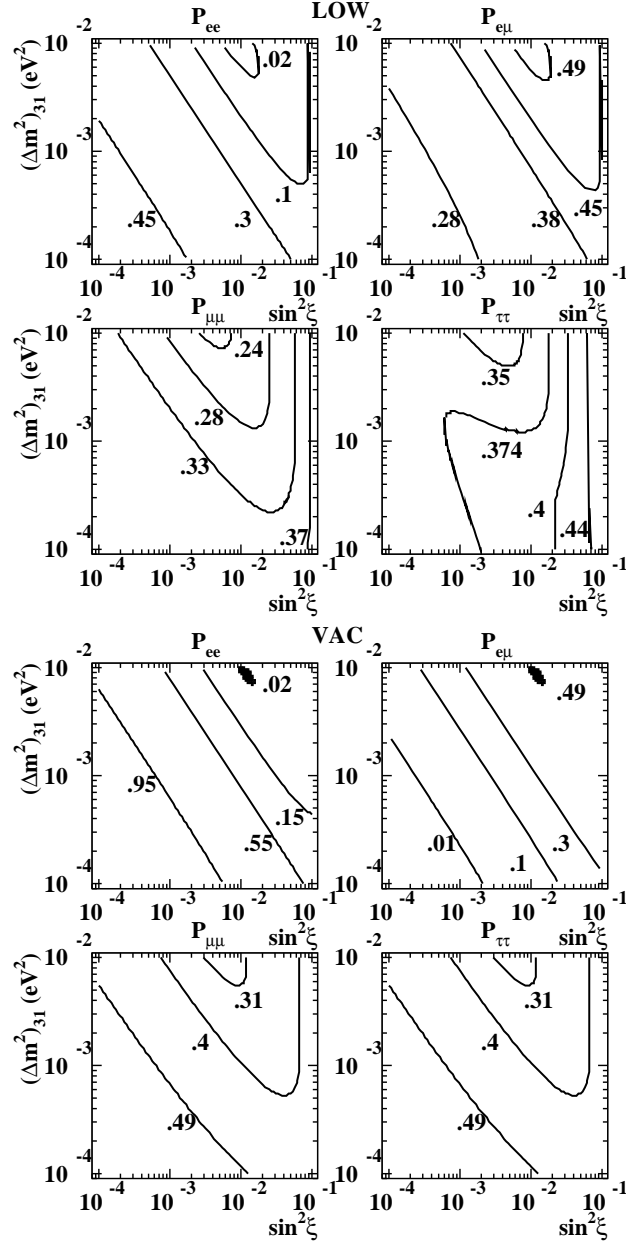


Figure 5: Constant $P_{\alpha\beta}$ contours in the $(\Delta m_{31}^2 \times \sin^2 \xi)$ -plane, at LOW (top) and VAC (bottom) (see text).

$$b_\mu^2 = a_\tau^2 = 0.5(1 - 2\sqrt{P_c^L(1 - P_c^L)}), \quad (4.5)$$

$$a_\mu b_\mu = -a_\tau b_\tau = 0.5(1 - 2P_c^L), \quad (4.6)$$

and

$$\begin{aligned} P_{(\mu\mu,\tau\tau)} &= \frac{1}{2}(1 - U_{(\mu,\tau)3}^2) \pm \sqrt{P_c^L(1 - P_c^L)}(U_{(\mu,\tau)1}^2 - U_{(\mu,\tau)2}^2) \\ &\pm (1 - 2P_c^L)U_{(\mu,\tau)1}U_{(\mu,\tau)2} \cos\left(\frac{\Delta m_{21}^2 x}{2E_\nu}\right). \end{aligned} \quad (4.7)$$

At both LMA and SMA, the oscillatory term averages out to zero, while at VAC $\cos\left(\frac{\Delta m_{21}^2 x}{2E_\nu}\right) = 1$. It is only at LOW that the oscillatory term is nontrivial, as was mentioned in the analogy between the situation at hand and the solutions to the solar neutrino puzzle.

Furthermore, at SMA, $1 - P_c^L$ is tiny (see Fig. 3), so it is fair to approximate $P_{\mu\mu} \simeq P_{\tau\tau} \simeq 0.5(1 - 0.5 \times 0.99) \simeq 0.25$, in agreement with Fig. 4(bottom). At LMA, it is fair to approximate $\sin^2 \xi = 0$. In this limit, $U_{\mu 1}^2 - U_{\mu 2}^2 \simeq -0.5 \cos 2\omega + \sin 2\omega \sin \xi$, while $U_{\tau 1}^2 - U_{\tau 2}^2 \simeq -0.5 \cos 2\omega - \sin 2\omega \sin \xi$. Therefore, because $\cos 2\omega = 0.6 > 0$, $P_{\mu\mu}$ is significantly less than $P_{\tau\tau}$, since $\sqrt{P_c^L(1 - P_c^L)}$ is nonnegligible. Roughly, $P_{\mu\mu} \simeq 0.15$ and $P_{\tau\tau} \simeq 0.4$, using the approximations above. Again, there is agreement with Fig. 4(top).

In order to understand the behaviour at LOW and VAC, one should take advantage of the fact that $1 - P_c^L \rightarrow \sin^2 \omega$. In this case, it proves more advantageous to use the second form of Eq. (3.13) in order to express all $P_{\alpha\beta}$

$$\begin{aligned} P_{ee} &= P_2^H \cos^2 \xi + P_3^H \sin^2 \xi - (\text{Osc})_{ee}, \\ P_{e\mu} &= (P_2^H \sin^2 \xi + P_3^H \cos^2 \xi) \sin^2 \theta - (\text{Osc})_{e\mu}, \\ P_{\mu\mu} &= (\cos^2 \theta + \sqrt{P_3^H} \sin \xi \sin^2 \theta)^2 + P_2^H \cos^2 \xi \sin^4 \theta - (\text{Osc})_{\mu\mu}, \\ P_{\tau\tau} &= (\sin^2 \theta + \sqrt{P_3^H} \sin \xi \cos^2 \theta)^2 + P_2^H \cos^2 \xi \cos^4 \theta - (\text{Osc})_{\tau\tau}, \end{aligned} \quad (4.8)$$

where

$$(\text{Osc})_{\alpha\beta} = 4a_\alpha b_\alpha U_{\beta 1} U_{\beta 2} \sin^2 \left(\frac{\Delta m_{12}^2 x}{4E_\nu} \right) \quad (4.9)$$

are the oscillatory terms. When $L_{\text{osc}}^{21} \gg 1$ a.u., the oscillatory terms are zero, and $P_{\alpha\beta}$ are particularly simple. Note that on this limit many simplifications

happen: $P_{\alpha\beta}$ is independent of ω and Δm_{21}^2 , and $P_{\mu\mu} = P_{\tau\tau}$ if $\sin^2 \theta = \cos^2 \theta$, as can be observed in Fig. 5(bottom). A very important fact is that, when the oscillatory terms are neglected, $2P_{e\mu} = 1 + P_{\tau\tau} - P_{\mu\mu} - P_{ee}$, as one may easily verify directly. As argued before, when this condition is satisfied, $P_{\alpha\beta} = P_{\beta\alpha}$. This is not the case in the presence of nonnegligible oscillation effects or when $P_c \neq \cos^2 \omega$. Both statements are trivial to verify directly. For example,

$$4a_e b_e U_{\mu 1} U_{\mu 2} = P_2^H \sin 2\omega \left[\sin 2\omega \left(\sin^2 \xi \sin^2 \theta - \cos^2 \theta \right) - \sin \xi \sin 2\theta \cos 2\omega \right] \quad (4.10)$$

while

$$4a_\mu b_\mu U_{e 1} U_{e 2} = \cos^2 \xi \sin 2\omega \left[\sin 2\omega \left(P_3^H \sin^2 \theta - \cos^2 \theta \right) - \sqrt{P_3^H} \sin 2\theta \cos 2\omega \right], \quad (4.11)$$

so $\text{Osc}_{e\mu} \neq \text{Osc}_{\mu e}$.

Figs. 6 and 7 depict $P_{\alpha\beta}$ as a function of $\sin^2 \theta$ at LMA and SMA, and at LOW and VAC, respectively. In these figures, all $P_{\alpha\beta}$ are plotted, in order to illustrate that $P_{\alpha\beta} \neq P_{\beta\alpha}$ at LMA, SMA and VAC. Note that at LMA and SMA, the difference comes from the fact that $P_3^H \neq \sin^2 \xi$ and $P_c^L \neq \cos^2 \omega$. At LOW, $P_c^L \simeq \cos^2 \omega$, but $P_3^H \neq \sin^2 \xi$ and nontrivial oscillatory terms render $P_{\alpha\beta} \neq P_{\beta\alpha}$. At VAC, even though $P_3^H \neq \sin^2 \xi$, $P_{\alpha\beta} = P_{\beta\alpha}$ because $P_c^L = \cos^2 \omega$ and because “1-2” oscillations don’t have “time” to happen.

From Eqs. (4.8) one can roughly understand the dependency of $P_{\alpha\beta}$ on $\sin^2 \theta$. Obviously P_{ee} does not depend on θ (by the very form of the MNS matrix, Eq. (3.1)), while $P_{e\mu}$ ($P_{e\tau}$) depends almost exclusively on $\sin^2 \theta$ ($\cos^2 \theta$). This is guaranteed by the fact that $P_3^H \gg P_2^H$ even at LMA and LOW, when one expects the interference terms to play a significant role. It is also worthwhile to note that, as expected, at VAC and SMA the curves are very similar, a behaviour that can be understood from earlier discussions.

Finally, Fig. 8 depicts constant $P_{\alpha\beta}$ contours in the $(\Delta m_{21}^2 \times \sin^2 \omega)$ -plane, at ATM. In light of the previous discussions, the shapes and forms can be readily understood. First note that the shapes of the constant P_{ee} and $P_{e\mu}$ regions resemble those of the pure vacuum oscillations depicted in Fig. 1, with two important differences. First, the constant values of the contours are quite different. For example, P_{ee} varies from a few percent to less than 15%, while in the case of pure vacuum oscillations, P_{ee} varies from 30% to 100%. This can be roughly understood numerically by noting that $P_{(ee,e\mu)} \simeq P_2^H P_{(ee,e\mu)}^{\text{vac}}$ (remember that $P_2^H = 1 - P_3^H \simeq 0.13$ when averaged over the energy range of interest). Second, at high Δm_{21}^2 , the regions are distorted. This is due

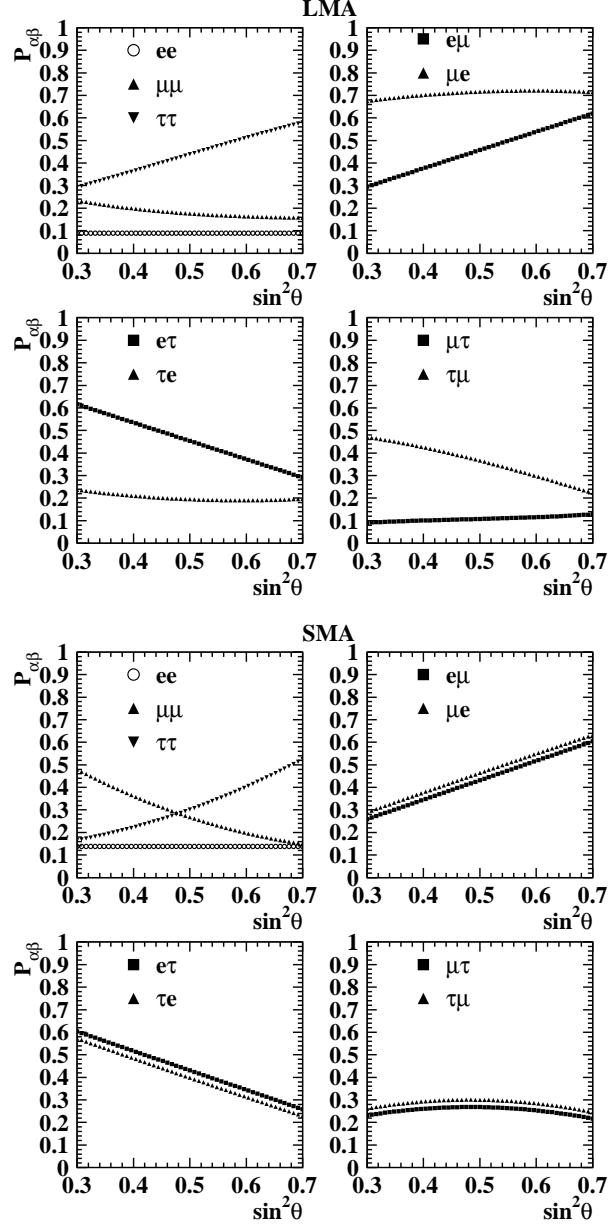


Figure 6: $P_{\alpha\beta}$ as a function of $\sin^2 \theta$, at LMA (top) and SMA (bottom) (see text).

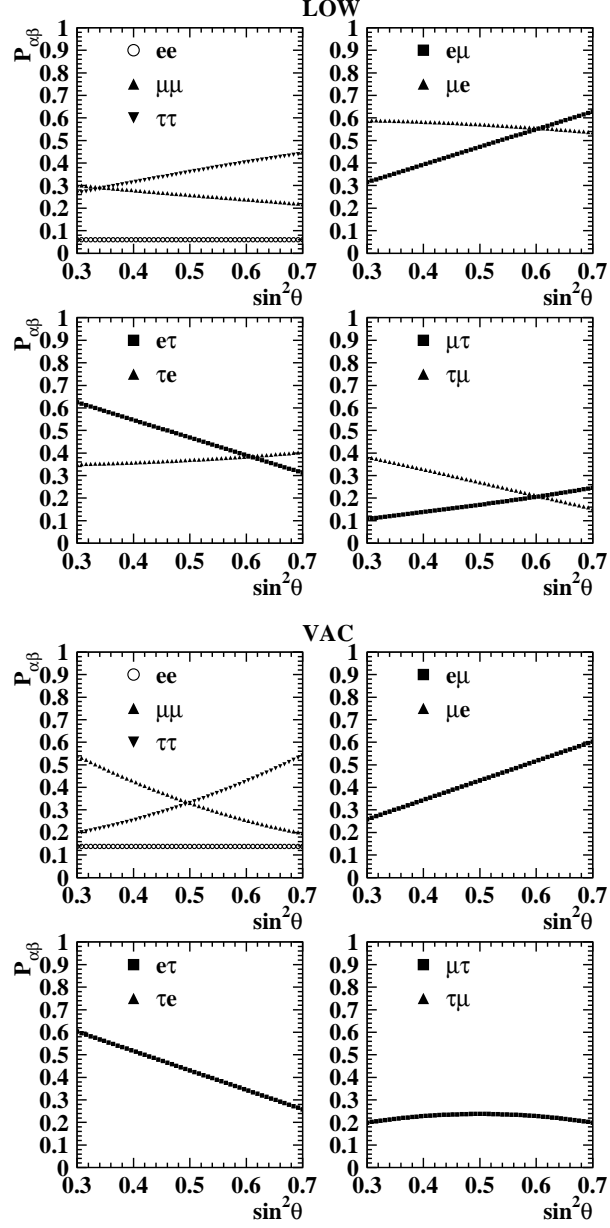


Figure 7: $P_{\alpha\beta}$ as a function of $\sin^2\theta$, at LOW (top) and VAC (bottom) (see text).

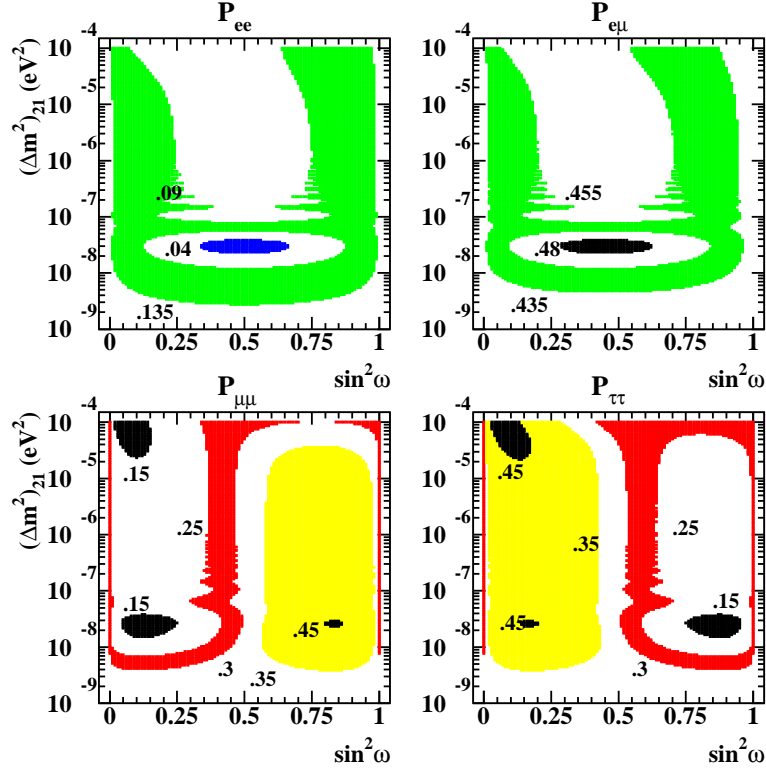


Figure 8: Constant $P_{\alpha\beta}$ contours in the $(\Delta m^2_{21} \times \sin^2 \omega)$ -plane, at ATM (see text).

to nontrivial matter effects in the “ $M - L$ ” system. Note that the contours follow the constant $1 - P_c^L$ curves depicted in Fig. 3.

The $P_{\mu\mu}$ and $P_{\tau\tau}$ contours are a lot less familiar, and require some more discussion. Many features are rather prominent. For example, the plane is roughly divided into a $\sin^2 \omega > 0.5$ and $\sin^2 \omega < 0.5$ structure, and large (small) values of $P_{\mu\mu}$ ($P_{\tau\tau}$) are constrained to the $\sin^2 \omega > 0.5$ half, and vice-versa. Also, there is a rough $P_{\mu\mu}(\omega) \leftrightarrow P_{\tau\tau}(\pi/2 - \omega)$ symmetry in the picture, which was present in the pure vacuum case (see Fig. 1). This symmetry is absent for large values of Δm^2_{21} , similar to what happens in the case of P_{ee} , and is due, as mentioned in the previous paragraph, to the fact that P_c^L is significantly different from $\cos^2 \omega$ in this region.

The other features are also fairly simple to understand, and are all due to fact that $P_3^H \gg \sin^2 \xi$. It is convenient to start the discussion in the limit

when $L_{21}^{\text{osc}} \gg 1$ a.u. (the very small Δm_{21}^2 region). As was noted before, $P_{\alpha\beta}$ are given by Eq. (4.8) where the $\text{Osc}_{\alpha\beta}$ terms vanish. It is therefore easy to see that $P_{\alpha\beta}$ do not depend on ω or Δm_{21}^2 (as mentioned before), and furthermore it is trivial to compute the value of $P_{\alpha\beta}$ given that we are at ATM and that $P_3^H \simeq 0.87$. The next curious feature is that there is a “band” around $\sin^2 \omega = 1/2$ where $P_{\mu\mu} \simeq P_{\mu\mu}(L_{21}^{\text{osc}} \rightarrow \infty)$. The same is true of $P_{\tau\tau}$. This is due to the fact that, around $\sin^2 \omega \simeq 1/2$, $a_\mu b_\mu$ and $a_\tau b_\tau$ vanish when P_3^H is large. In the limit $P_3^H = 1$ one can use Eq.(4.6) and note that indeed both $a_\mu b_\mu$ and $a_\tau b_\tau$ vanish at $P_c^L = 1/2$. However, for values of $\Delta m_{21}^2 \lesssim 10^{-7} \text{ eV}^2$ $P_c^L \simeq \cos^2 \omega$, which explains the band around $\omega \simeq \pi/4$. Slight distortions are due to the fact that $P_3^H \neq 1$, and are easily computed from the exact expressions.

Again in the limit $P_3^H = 1$, $P_c^L = \cos^2 \omega$, the coefficient of the $\cos\left(\frac{\Delta m_{21}^2 x}{2E_\nu}\right)$ term Eq. (4.7) is

$$\pm \frac{1}{2}(1 - 2 \cos^2 \omega) \left(-\frac{1}{2} \sin 2\omega \mp 0.1 \cos 2\omega \right), \quad (4.12)$$

if $\sin^2 \xi$ terms are neglected. The $+$, $-$ signs are for $P_{\mu\mu}$ while the $-$, $+$ signs for $P_{\tau\tau}$. It is trivial to verify numerically (if a little tedious) that the $P_{\mu\mu}$ term has a maximum at $\sin^2 \omega \simeq 0.1$ and a minimum at $\sin^2 \omega \simeq 0.8$. For $P_{\tau\tau}$ the maximum (minimum) is at $\sin^2 \omega \simeq 0.9(0.2)$. It is important to comment that the minima are negative numbers. On the other hand, from Fig. 1 (as mentioned before) it is easy to see that $\cos\left(\frac{\Delta m_{21}^2 x}{2E_\nu}\right)$ is minimum for $\Delta m_{21}^2 \simeq 2 \times 10^{-8} \text{ eV}^2$ (this is where all $P_{\alpha\alpha}$ are maximally suppressed in Fig. 1). Combining both informations, it is simple to understand the maxima/minima of $P_{\mu\mu}$ and $P_{\tau\tau}$ at $\Delta m_{21}^2 \simeq 2 \times 10^{-8} \text{ eV}^2$: Minima occur when the coefficient is maximum (*e.g.*, at $\sin^2 \omega \simeq 0.1$ for $P_{\mu\mu}$) while maxima occur when the coefficient is minimum (*e.g.*, at $\sin^2 \omega \simeq 0.8$ for $P_{\mu\mu}$). A description of what has happened is the following: The matter effects “compress” the constant $P_{\mu\mu}$ ($P_{\tau\tau}$) contours from the pure vacuum oscillation case (presented in Fig. 1) to the $\sin^2 \omega < 1/2$ ($> 1/2$) half of the plane, and a new region “appears” on the other half. This other region is characterised by negative values to the coefficients of the oscillatory terms, which are not attainable in the case of pure vacuum oscillations (see Eq. (4.2)).

At last, the contours in the region where the oscillatory effects average out, $P_{\mu\mu}$ and $P_{\tau\tau}$ are also best understood from Eq. (4.7) and the paragraphs which follow it, in the limit that $\cos\left(\frac{\Delta m_{21}^2 x}{2E_\nu}\right) \rightarrow 0$. It is simple to see, for

example, that $P_{\mu\mu} < P_{\tau\tau}$ if $\cos 2\omega > 0$ ($\sin^2 \omega > 1/2$), while the situation is reversed if $\cos 2\omega < 0$. This is indeed what one observes in Fig. 8.

4.3 “Inverted” Neutrino Hierarchy

Here I turn to the case of an “inverted” neutrino hierarchy, namely $\Delta m_{31}^2 < 0$. Currently, there is no experimental hint as to what the sign of Δm_{31}^2 should be, so there is no reason to believe that the “normal” hierarchy is to be preferred over the “inverted” hierarchy. Indeed, even from a theoretical/model building point of view, there are no strong reasons for or against a particular neutrino mass hierarchy [41].

The discussion will be restricted to $\Delta m_{21}^2 > 0$ for two reasons. First, the $\Delta m_{21}^2 < 0$ can be approximately read off from the $\Delta m_{21}^2 > 0$ case by changing $\omega \rightarrow \pi/2 - \omega$, as mentioned before. Second, and most important, there is some experimental hints as to what is the sign of Δm_{21}^2 [12, 11]. For example, the SMA solution only exists for one sign of Δm_{21}^2 , while the LMA and LOW solutions prefer one particular sign. Even in the case of VAC there is the possibility of obtaining information concerning the sign of Δm_{21}^2 from solar neutrino data [40]. Therefore, the notation introduced in the beginning of this section (ATM, SMA, LMA, LOW, VAC) still applies, and one should simply remember that here $\Delta m_{31}^2 < 0$.

As advertised, the largest effect of $\Delta m_{31}^2 < 0$ is the typical values of P_c^H . From Eq. (2.12), keeping in mind that here γ is negative,

$$P_c^H = \frac{1 - e^{-|\gamma| \cos^2 \xi}}{1 - e^{-|\gamma|}}, \quad (4.13)$$

where γ is given by Eq. (2.13) with $\Delta m^2 \rightarrow \Delta m_{31}^2$. Since $|\gamma| \gg 1$ (see Eq. (2.13)), $P_c^H = 1$ for all values of Δm_{31}^2 and $\sin^2 \xi$ of interest. Indeed, this is true for any value of $\sin^2 \xi$ as long as $\Delta m_{31}^2 \gg 10^{-6} \text{ eV}^2$. This is to be contrasted to the normal hierarchy case, when there is always some value of $\sin^2 \xi$ (which is a function of Δm_{31}^2) below which P_c deviates significantly from its adiabatic limit.

All of the Δm_{31}^2 dependency of $P_{\alpha\beta}$ is therefore encoded in ξ_M . However, in the case $\Delta m_{31}^2 < 0$ it is trivial to show that $-1 < \cos 2\xi_M < -\cos 2\xi$, where the upper bound is reached in the limit $|\Delta m_{31}^2/2E_\nu| \gg A$ (this has been mentioned before. The minus sign takes care of the “unorthodox” $P_c \rightarrow 1$ adiabatic limit). Since one is interested in $\sin^2 \xi < 0.1$ ($-\cos 2\xi < -0.8$), the

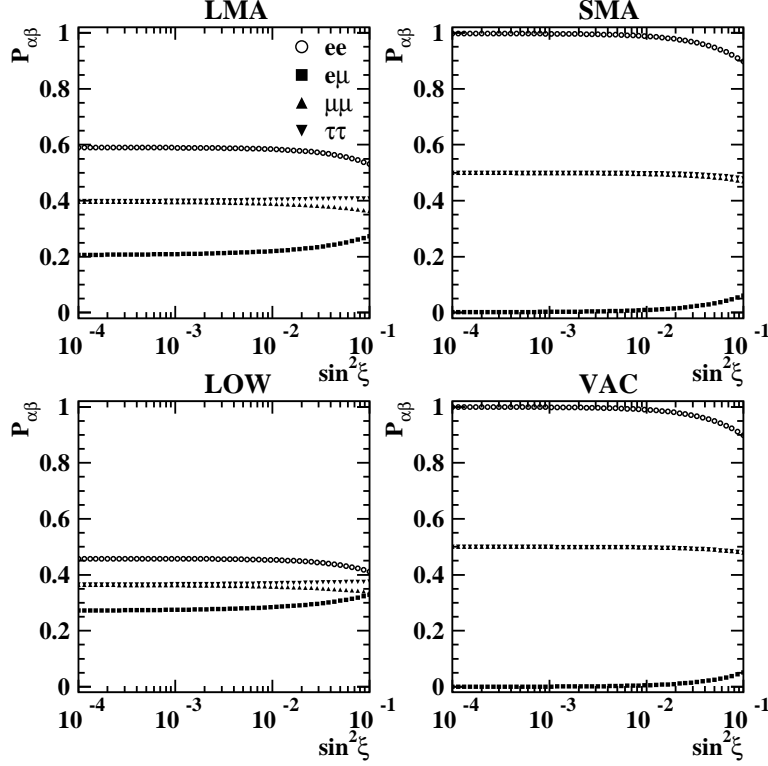


Figure 9: $P_{\alpha\beta}$ as a function of $\sin^2 \xi$, at LMA, SMA, LOW, and VAC (see text), for $\Delta m_{31}^2 < 0$.

range for ξ_M is rather limited, and therefore any Δm_{31}^2 effects are bound to be very small. Larger Δm_{31}^2 effects are expected for larger $\sin^2 \xi$.

In light of this, Fig. 9 depicts $P_{\alpha\beta}$ and $P_{e\mu}$ as a function of $\sin^2 \xi$ at the various points (LMA, SMA, LOW, VAC), for $\Delta m_{31}^2 = -3 \times 10^{-3} \text{ eV}^2$ and $\sin^2 \theta = 0.5$.

It is interesting to compare the results presented here with the pure vacuum case. In the limit $P_2^H = 1$

$$P_{ee} = \cos^2 \xi \left[P_c^L \cos^2 \omega + (1 - P_c^L) \sin^2 \omega + \sqrt{P_c(1 - P_c^l)} \sin 2\omega \cos \left(\frac{\Delta m_{21}^2 L}{2E_\nu} \right) \right], \quad (4.14)$$

while the pure vacuum result in the same region of the parameter space is

$$P_{ee}^{\text{vac}} = \cos^4 \xi \left[\cos^4 \omega + \sin^4 \omega + 2 \sin^2 \omega \cos^2 \omega \cos \left(\frac{\Delta m_{21}^2 L}{2E_\nu} \right) \right] + \sin^4 \xi. \quad (4.15)$$

In the limit $P_c^L = \cos^2 \omega$, the difference

$$P_{ee} - P_{ee}^{\text{vac}} = \left(P_{ee}^{2\nu, \text{vac}} \right) \cos^2 \xi \sin^2 \xi - \sin^4 \xi, \quad (4.16)$$

where $P_{ee}^{2\nu, \text{vac}}$ is the electron neutrino survival probability in the two-flavour case with $\Delta m^2 = \Delta m_{21}^2$ and vacuum mixing angle ω . This difference vanishes at $\sin^2 \xi = 0$, and $\sin^2 \xi = \frac{P_{ee}^{2\nu, \text{vac}}}{1 + P_{ee}^{2\nu, \text{vac}}}$, (which is between 0 and 0.5). Furthermore, it is a convex function of $\sin^2 \xi$, which means that P_{ee} is *larger* than the pure vacuum case for values of $\sin^2 \xi < \frac{P_{ee}^{2\nu, \text{vac}}}{1 + P_{ee}^{2\nu, \text{vac}}}$. Away from the limit $P_c^L = \cos^2 \omega$, keeping in mind that the oscillatory terms average out, P_{ee} is still larger than the pure vacuum case if $\cos^2 \omega > \sin^2 \omega$ since $P_c^L \leq \cos^2 \omega$, as one can easily verify.

Also, in the limit $P_2^H = 1$, $\sin^2 \theta = 1/2$,

$$P_{\mu\mu} = \frac{1}{2} \left[(1 - P_c^L) U_{\mu 1}^2 + P_c^L U_{\mu 2}^2 + U_{\mu 3}^2 + 2 \sqrt{P_c^L (1 - P_c^L)} U_{\mu 1} U_{\mu 2} \cos \left(\frac{\Delta m_{21}^2 L}{2E_\nu} \right) \right]. \quad (4.17)$$

The same expression applies for $P_{\tau\tau}$ with $U_{\mu i} \rightarrow U_{\tau i}$. This is a consequence of $\sin^2 \theta = \cos^2 \theta$. Furthermore, in the limit $\sin^2 \xi \rightarrow 0$ (and for $\sin^2 \theta = \cos^2 \theta$), $U_{\mu i} = U_{\tau i}$, which explains why $P_{\mu\mu} = P_{\tau\tau}$ for $\sin^2 \xi \lesssim 10^{-2}$. At VAC this equality remains for all values of $\sin^2 \xi$. The reason for this is that, at VAC, the expression simplifies tremendously and $P_{\mu\mu} = P_{\tau\tau} = \frac{1}{4} (1 + \cos^2 \xi)$. In the same region of the parameter space, the pure vacuum oscillation case yields $P_{\mu\mu}^{\text{vac}} = P_{\tau\tau}^{\text{vac}} = \frac{1}{2} \cos^4 \xi - \cos^2 \xi + 1$. Note that, in this region of the parameter space $P_{\mu\mu}^{\text{vac}} \geq P_{\mu\mu}$, the inequality being saturated at $\cos^2 \xi = 1$.

The same result also applies (approximately) at SMA, since the oscillatory terms are proportional to $\sqrt{P_c^L (1 - P_c^L)}$ and $1 - P_c^L$ is very small at SMA (see Fig 3). The equality $P_{\mu\mu} = P_{\tau\tau}$ is broken at larger values of $\sin^2 \xi$ because $P_c^L \neq \cos^2 \omega$ at SMA.

It remains to discuss how $P_{\mu\mu}$ and $P_{\tau\tau}$ diverge from the pure vacuum case at LMA and LOW. In the limit $P_c^L = \cos^2 \omega$, and averaging out the

oscillatory terms,

$$P_{\mu\mu} - P_{\mu\mu}^{\text{vac}} = \frac{\sin \xi}{2} \left[\sin \xi \left(U_{\mu 3}^2 - (\cos^2 \omega U_{\mu 1}^2 + \sin^2 \omega U_{\mu 2}^2) \right) - \sin 2\omega (U_{\mu 1}^2 - U_{\mu 2}^2) \right]. \quad (4.18)$$

This difference goes to zero as $\sin^2 \xi \rightarrow 0$. This is to be expected, since in this limit the difference of P_2^H and $\cos^2 \xi$ disappears. For small values of $\sin^2 \xi$, the last term in Eq. 4.18 dominates, and, as discussed before, $U_{\mu 1}^2 - U_{\mu 2}^2 = -0.5 \cos 2\omega + O(\sin \xi)$. Therefore, $P_{\mu\mu} - P_{\mu\mu}^{\text{vac}} > 0$ (< 0) for $\cos 2\omega > 0$ (< 0). The expression for $P_{\tau\tau}$ can be obtained from Eq.(4.18) by replacing $U_{\mu i} \rightarrow U_{\tau i}$ and changing the sign of the last term. Therefore, since $U_{\tau 1}^2 - U_{\tau 2}^2 = -0.5 \cos 2\omega + O(\sin \xi)$, $P_{\tau\tau} - P_{\tau\tau}^{\text{vac}} > 0$ (< 0) for $\cos 2\omega < 0$ (> 0). When the oscillatory terms do not average out, it is easy to verify explicitly that the behaviour of the oscillatory terms follows the behaviour of the average terms, discussed above, and the inequalities obtained above still apply.

The situation, however, changes, when $P_c^L \neq \cos^2 \omega$, *i.e.*, when matter effects due to the “M-L” system are relevant. In this region, a behaviour similar to the one observed in the “normal” hierarchy case is expected, since $\Delta m_{21}^2 > 0$. Fig. 10 depicts constant $P_{\alpha\beta}$ contours in the $(\Delta m_{21}^2 \times \sin^2 \omega)$ -plane. One should be able to see upon close inspection that the region $P_{ee} < 30\%$ is smaller in Fig. 10 than the same region in the pure vacuum oscillation case, Fig 1. Also, the constant $P_{\mu\mu}$ ($P_{\tau\tau}$) contours are shifted to larger (smaller) values of $\sin^2 \omega$. The other prominent (and expected, as mentioned above) feature is the distortion of the contours at large values of Δm_{21}^2 . This behaviour is similar to the one observed in Fig. 8.

I conclude this subsection with a comment on antineutrinos. As discussed previously, $P_{\bar{\alpha}\bar{\beta}}(\Delta m_{21}^2, \Delta m_{31}^2) = P_{\alpha\beta}(-\Delta m_{21}^2, -\Delta m_{31}^2)$, such that the “normal” hierarchies yield “inverted” hierarchy results for antineutrinos, and vice-verse. One cannot, however, apply Fig. 8 and Fig. 10 for the antineutrinos because both Δm_{ij}^2 have to change sign, not just Δm_{31}^2 . Qualitatively, however, it is possible to understand the constant $P_{\bar{\alpha}\bar{\beta}}$ contours by examining figures Fig. 8 and Fig. 10 reflected in a mirror positioned at $\sin^2 \omega = 0.5$, meaning that $P_{\bar{\alpha}\bar{\beta}}(\sin^2 \omega, \Delta m_{31}^2) \simeq P_{\alpha\beta}(\cos^2 \omega, -\Delta m_{31}^2)$. The equality is not complete because one is also required to exchange $\theta \rightarrow \pi - \theta$, as mentioned earlier.

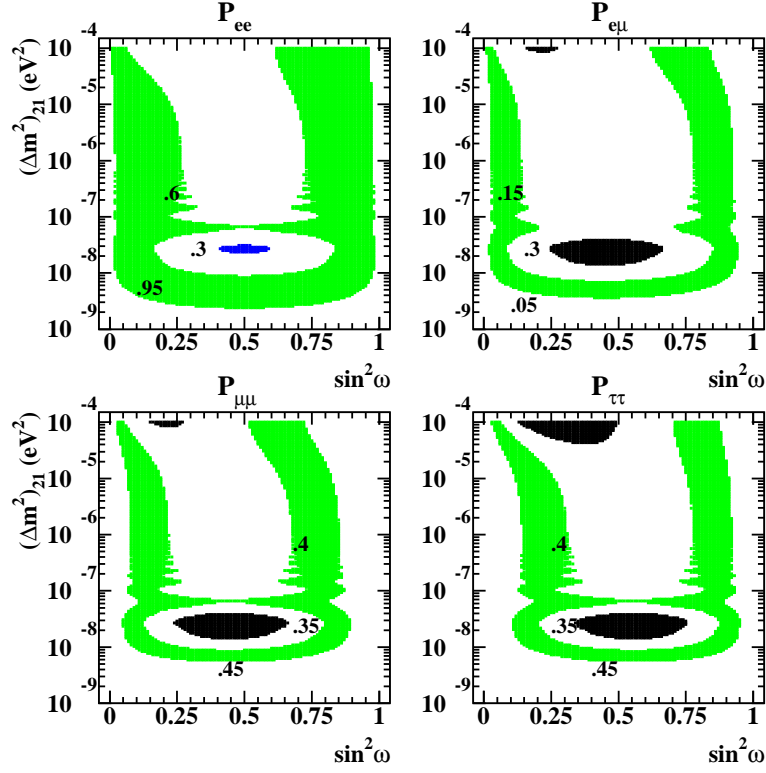


Figure 10: Constant $P_{\alpha\beta}$ contours in the $(\Delta m_{21}^2 \times \sin^2 \omega)$ -plane, at ATM (see text), for $\Delta m_{31}^2 < 0$.

4.4 Higher Neutrino Energies

As the average neutrino energy increases, the values of $P_{\alpha\beta}$ start to resemble more the pure vacuum case. This is easy to see from Figs. 2 and 3. Any deviation of $1 - P_c^L$ from $\sin^2 \omega$ goes away even at LMA for $E_\nu \simeq 50$ GeV, while “H-M” effects remain important up to $E_\nu \simeq 1$ TeV, even though quantitatively the effect decreases noticeably. This can be illustrated by the value of P_3^H at ATM, for example, which drops from 0.87 for energies which range from 1 to 5 GeV (see the previous subsections) to 0.058, for energies which range from 100 to 110 GeV.

Furthermore, all L_{ij}^{osc} increase as the energy increases, for fixed values of Δm_{ij}^2 . Therefore, LOW becomes indistinguishable from VAC at $E_\nu \simeq 100$ GeV. For $O(\text{TeV})$ neutrinos the sensitivity to Δm_{21}^2 remains only for its highest allowed values, while one should start worrying about nontrivial

oscillatory effects due to L_{31}^{osc} .

The case of higher energy neutrinos contains a more serious complications: neutrino absorption inside the Sun. As the neutrino energy increases, one has to start worrying about the fact that absorptive neutrino interactions can take place. According to [42], for neutrinos produced in the Sun's core, absorption becomes important for $E_\nu \gtrsim 200$ GeV. In this case, ν_e and ν_μ interact with nuclear matter and produce electrons and muons, respectively. The former are capture and “lost” inside the Sun, while the latter stop before decaying into low energy neutrinos. The case of ν_τ -Sun interactions is more interesting, because the τ -leptons produced via charged current interactions decay before “stopping”, yielding ν_τ 's with slightly reduced energies. Therefore, it is possible to get a flux of very high energy initial state τ -neutrinos but not muon or electron-type neutrinos. Such effects have been studied for high energy galactic neutrinos traversing the Earth [43].

The effect of neutrino oscillations inside the Sun in the presence of non-negligible neutrino absorption is certainly of great interest but is beyond the scope of this paper.

5 Conclusions

The oscillation probability of $O(\text{GeV})$ neutrinos of all flavours produced in the Sun's core has been computed, including matter effects, which are, in general, nontrivial.

In particular, it was shown that, unlike the two-flavour oscillation case, in the three-flavour case the probability of a neutrino produced in the flavour eigenstate α to be detected as a flavour eigenstate β ($P_{\alpha\beta}$) is (in general) different from $P_{\beta\alpha}$, even if the CP -violating phase of the MNS matrix vanishes. This is, of course, expected since Sun–neutrino interactions explicitly break T -invariance. Indeed, it is the case of two-flavour oscillations which is special, in the sense that the number of independent oscillation probabilities is too small because of unitarity.

The results of a particular scan of the parameter space are presented in Sec. 4. In this case, special attention was paid to the regions of the parameter space which are preferred by the current experimental situation.

It turns out that, in the case of a “normal” neutrino mass hierarchy, it is possible to suppress P_{ee} tremendously with respect to its pure vacuum oscillation values, by a mechanism that is similar to the well known MSW

effect in the case of two-flavour oscillations: the parameters are such that electron-type neutrinos produced in the Sun’s core exit the Sun (almost) as pure mass eigenstates, and the ν_e component of this eigenstate is small. Both $P_{\mu\mu}$ and $P_{\tau\tau}$ can be significantly suppressed, and the constant $P_{\mu\mu}$ and $P_{\tau\tau}$ contours as a function of the “solar” angle and the smaller mass-squared differences are nontrivial. One important feature is that when $P_{\mu\mu}$ is significantly suppressed, $P_{\tau\tau}$ is not, and vice-versa. One consequence of this is that, for some regions of the parameter space, it is possible to have an enhancement of ν_τ ’s detected in the Earth with respect to the number of ν_μ ’s (or vice-versa). This may have important implications for solar WIMP annihilation searches at neutrino telescopes, and will be studied in another opportunity. It is important to note that the effect of neutrino oscillations on the expected event rate at neutrino telescopes will depend on the expected production rate of individual neutrino species inside the Sun, which is, of course, model dependent.

In the case of an “inverted” mass hierarchy, the situation is very similar to the pure vacuum case, and no particular suppression of any $P_{\alpha\alpha}$ is possible. Indeed, for a large region of the parameter space P_{ee} is in fact enhanced, a feature which is also observed in the two-flavour case [39].

The case of higher energy neutrinos was very briefly discussed, and the crucial point is to note that, for neutrino energies above a few hundred GeV, the absorption of neutrinos by the Sun becomes important. The study of absorption effects is beyond the scope of this paper.

Finally, it is important to reemphasise that the values of $P_{\alpha\beta}$ computed here are to be understood as if they were evaluated at the Earth’s surface. No Earth-matter effects have been included. It is possible that Earth-matter effects are important, especially the ones related to Δm_{31}^2 , in the advent that $U_{e3}^2 \equiv \sin^2 \xi$ turns out to be “large.”

Acknowledgements

I would like to thank John Ellis for suggesting the study of GeV solar neutrinos, and for many useful discussions and comments on the manuscript. I also thank Amol Dighe and Hitoshi Murayama for enlightening discussions and for carefully reading this manuscript and providing useful comments.

References

- [1] Super-Kamiokande Collaboration (Y. Fukuda *et al.*), *Phys. Rev. Lett.* **81**, 1562 (1998), hep-ex/9807003.
- [2] N. Fornengo, M.C. Gonzalez-Garcia, and J.W.F. Valle, FTUV-00-13, IFIC-00-14, hep-ph/0002147.
- [3] B.T. Cleveland *et al.*, *Astrophys. J.* **496**, 505 (1998).
- [4] KAMIOKANDE Collaboration (Y. Fukuda *et al.*), *Phys. Rev. Lett.* **77**, 1683 (1996).
- [5] GALLEX Collaboration (W. Hampel *et al.*), *Phys. Lett.* **B447**, 127 (1999).
- [6] SAGE Collaboration (J.N. Abdurashitov *et al.*), *Phys. Rev.* **C 59**, 2246 (1999); SAGE Collaboration (J.N. Abdurashitov *et al.*), astro-ph/9907113.
- [7] Super-Kamiokande Collaboration (Y. Fukuda *et al.*), *Phys. Rev. Lett.* **81**, 1158 (1998), hep-ex/9805021.
- [8] J.N. Bahcall, S. Basu, and M.H. Pinsonneault, *Phys. Lett.* **B433**, 1 (1998), astro-ph/9805135.
- [9] J.N. Bahcall, P.I. Krastev, and A.Yu. Smirnov, *Phys. Rev.* **D 58**, 096016 (1998), hep-ph/9807216.
- [10] M.C. Gonzalez-Garcia *et al.*, FTUV-99-41, hep-ph/9906469.
- [11] A. de Gouvêa, A. Friedland, and H. Murayama, UCB-PTH-00-03, hep-ph/0002064.
- [12] G.L. Fogli *et al.*, BARI-TH-365-99, hep-ph/9912231.
- [13] B. Pontecorvo, *Zh. Eksp. Teor. Fiz.* **33**, 549 (1957).
- [14] Z. Maki, M. Nakagawa, and S. Sakata, *Prog. Theor. Phys.* **28**, 870 (1962).
- [15] L. Wolfenstein, *Phys. Rev.* **D 17**, 2369 (1978);

- [16] S.P. Mikheyev and A.Yu. Smirnov, *Yad. Fiz. (Sov. J. of Nucl. Phys.)* **42**, 1441 (1985).
- [17] T.K. Kuo and J. Pantaleone, *Phys. Rev. Lett.* **57**, 1805 (1986); *Phys. Rev. D* **35**, 3432 (1987).
- [18] S.P. Mikheyev and A.Yu. Smirnov, *Phys. Lett. B* **200**, 560 (1987).
- [19] for a review, see G. Jungman, M. Kamionkowski, and K. Griest, *Phys. Rep.* **267**, 195 (1996).
- [20] AMANDA Collaboration (P. Askebjerg et al.), *Nucl. Phys. Proc. Suppl.* **77** 474, (1999).
- [21] BAIKAL Collaboration (V.A. Balkanov et al.), *Prog. Part. Nucl. Phys.* **40**, 391 (1998).
- [22] J. Ellis, R.A. Flores, and S.S. Masood, *Phys. Lett. B* **294**, 229 (1992).
- [23] T.K. Kuo and J. Pantaleone, *Phys. Rev.*, **D 37**, 298 (1988).
- [24] V. Barger, *et al.*, *Phys. Rev. D* **22**, 2718 (1980).
- [25] see, *e.g.*, A. De Rújula, M.B. Gavela, and P. Hernández, *Nucl. Phys. B* **547**, 21 (1999); V. Barger, S. Geer, and K. Whisnant, *Phys. Rev.*, **D 61**, 053004 (2000); A. Bueno, M. Campanelli, and A. Rubbia, ICARUS-TM-2000-01, hep-ph/0005007.
- [26] for a general and updated review see S.M. Bilenkii, C. Giunti, and W. Grimus, *Prog. Part. Nucl. Phys.* **43**, 1 (1999), hep-ph/9812360.
- [27] <http://www.sns.ias.edu/~jnb/>
- [28] S.T. Petcov, *Phys. Lett. B* **214**, 139 (1988).
- [29] S. Pakvasa and J. Pantaleone, *Phys. Rev. Lett.* **65**, 2479, (1990).
- [30] T. Kaneko, *Prog. Theor. Phys.* **78**, 532 (1987); S. Toshev, *Phys. Lett. B* **196**, 170 (1987); M. Ito, T. Kaneko, and M. Nakagawa, *Prog. Theor. Phys.* **79**, 13 (1988) [Erratum **79**, 555 (1988)].
- [31] S.T. Petcov, *Phys. Lett. B* **200**, 373 (1988).

- [32] P.I. Krastev and S.T. Petcov, *Phys. Lett. B* **207**, 64 (1988).
- [33] S.T. Petcov and J. Rich, *Phys. Lett. B* **224**, 426 (1989); J. Pantaleone, *Phys. Lett. B* **251**, 618 (1990).
- [34] M.V. Chizhov, IC-99-135, hep-ph/9909439.
- [35] Particle Data Group (C. Caso *et al.*), *Eur. Phys. J. C* **3**, 1 (1998).
- [36] Chooz Collaboration (M. Apollonio *et al.*), *Nucl. Phys. Proc. Suppl.* **77**, 159 (1999); F. Boehm *et al.*, STANFORD-HEP-00-03, hep-ex/0003022.
- [37] LSND Collaboration (C. Athanassopoulos *et al.*), *Phys. Rev. Lett.* **81**, 1774 (1998); *Nucl. Phys. Proc. Suppl.* **77**, 207 (1999).
- [38] J. Pantaleone, *Phys. Rev. D* **43**, 641 (1991).
- [39] A. de Gouvêa, A. Friedland, and H. Murayama, LBNL-44351, hep-ph/9910286.
- [40] A. Friedland, UCB-PTH-00-04, hep-ph/0002063.
- [41] For recent reviews see, *e.g.* R.N. Mohapatra, to appear in “Current Aspects of Neutrino Physics”, ed. by D. Caldwell, Springer-Verlag, 2000, hep-ph/9910365; S.M. Barr and I. Dorsner, BA-00-15, hep-ph/0003058.
- [42] R. Gandhi *et al.*, *Astropart. Phys.* **5**, 81 (1996).
- [43] S. Iyer, M.H. Reno, and I. Sarcevic, *Phys. Rev. D* **61**, 053003 (2000).